Supplemental Information

Role of Order in the Mechanism of Charge Transport across Single-Stranded and Double-Stranded DNA Monolayers in Tunnel Junctions

Nipun Kumar Gupta,[1,2†] Edward A. Wilkinson,[3†] Senthil Kumar Karuppannan,[1] Lily Bailey,[3] Ayelet Vilan,[4] Ziyu Zhang,[1] Dong-Chen Qi,[5] Anton Tadich,[6] Eimer M. Tuite,[7*] Andrew R. Pike,[7*] James H. R. Tucker,[3*] and Christian A. Nijhuis[1,2,8*]*

[1]Department of Chemistry, National University of Singapore, 3 Science Drive 3, Singapore 117543, Singapore.
[2]Centre for Advanced 2D Materials, National University of Singapore, 6 Science Drive 2, Singapore 117546, Singapore.
[3]School of Chemistry, University of Birmingham, Edgbaston, Birmingham, West Midlands B15 2TT, U.K
[4]Department of Chemical and Biological Physics, Weizmann Institute of Science, Rehovot 76100, Israel.
[5]Centre for Materials Science, School of Chemistry and Physics, Queensland University of Technology, Brisbane, Queensland 4001, Australia
[6]Australian Synchrotron Clayton, 800 Blackburn Rd Clayton, Victoria 3168, Australia.
[7]Chemistry-School of Natural and Environmental Sciences, Newcastle University, Newcastle upon Tyne, NE1 7RU (UK).
[8]Department of Molecules & Materials, MESA+ Institute for Nanotechnology, Faculty of Science and Technology, University of Twente, P.O. Box 217, 7500 AE Enschede, The Netherlands

[†]Authors contributed equally

*Author to whom correspondence should be addressed: c.a.nijhuis@utwente.nl, j.tucker@bham.ac.uk, eimer.tuite@newcastle.ac.uk, andrew.pike@newcastle.ac.uk, ayelet.vilan@weizmann.ac.il

Table of Contents

S1: Synthesis of Ferrocene Tag Precursor

General Instrumentation: ^{1}H NMR and ^{31}P NMR spectra were recorded on a Bruker AVIII 300 NMR spectrometer, recorded at 300 MHz. ^{13}C NMR spectra were recorded on a Bruker AVIII 400 spectrometer, recorded at 101 MHz. Mass spectrometry data was acquired by a Waters Xevo Micromass LCT Electro-spray Time–of–Flight (ES–TOF) mass spectrometer. FT–IR spectra were recorded using PerkinElmer 100FT–IR spectrometer at r.t. using ATR attachment. Melting points were carried out in triplicate and an average of the values recorded and reported as a range using Stuart SMP10 melting point apparatus.

Materials:

All reagents and solvents were purchased from Sigma-Aldrich, Acros Organics, Alfa Aesar, Fisher Scientific, VWR and LGC Genomics and used as received. Dry solvents were either purchased as such or obtained from a Pure Solv-MD solvent purification system and transported under an atmosphere of argon. Reactions using anhydrous solvents were performed in oven-dried glassware under an atmosphere of argon. Thin-layer chromatography (TLC) was performed on Merck silica gel 60 plates and visualised using short-wave UV light (254 nm). Flash column chromatography was performed using Merck silica 60.

Abbreviations:

DIPEA – *N*,*N*–diisopropylethylamine

DMAP – 4-dimethylaminopyridine

DMF – *N*,*N*-dimethylformamide

DMT – 4,4′-dimethoxytrityl

Fc – Ferrocene

TMEDA – *N*,*N*,*N*′,*N*′-tetramethylethylenediamine

THF – tetrahydrofuran

Synthetic Route:

The synthetic route followed to obtain the ferrocene phosphoramidite tag precursor is shown below (Scheme S1), which was adapted slightly from a literature procedure to obtain the same compound.[1]

The main difference was the bis-alkene reduction step, which was performed using H_2, catalysed by $Pd(OH)_2$ on carbon.

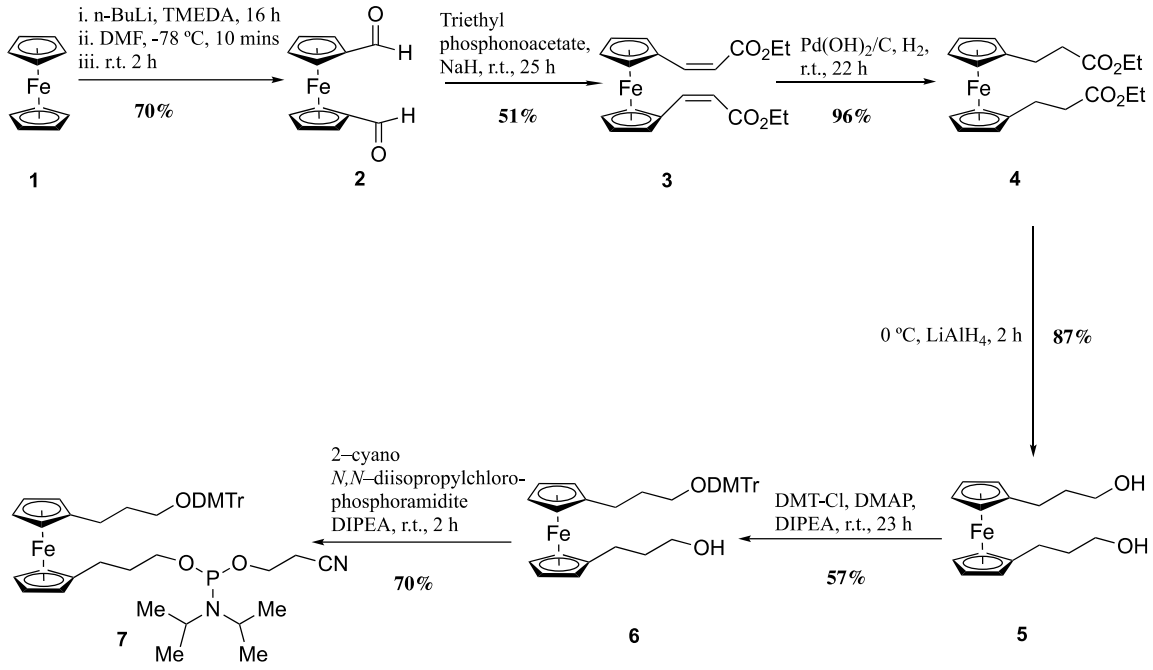

Scheme S1. Synthetic route to the ferrocene phosphoramidite tag precursor, compound **7**.

1,1'-Ferrocenedicarboxaldehye, compound 2

Ferrocene (3.0 g, 16.13 mmol, 1.0 equiv) was dissolved in anhydrous Et_2O (25 mL) under an argon atmosphere. TMEDA (5.77 mL, 38.7 mmol, 2.4 equiv.) was added to the mixture. *n*-BuLi (16.7 mL, 41.9 mmol, 2.6 equiv) was added dropwise and the reaction was stirred for 16 h. The reaction mixture was cooled to -78 °C and DMF (5.50 mL, 70.95 mmol, 3.3 equiv.) was added dropwise and the solution was stirred for 10 min. The solution was then warmed to room temperature over 30 min and stirred for a further 2 h. The reaction mixture was quenched with brine (20 mL) and the organic components were extracted with CH_2Cl_2 (3 × 20 mL). The organic components were dried over anhydrous $MgSO_4$ and filtered. The solvent was removed *in-vacuo* and the crude product was purified by column chromatography (silica gel, 1:1 ethyl acetate:hexane) to yield the product as a deep red solid (70%, 2.74 g, 11.3 mmol, R_f 0.57); MP: 151–152 ºC; ^{1}H NMR (300 MHz, $CDCl_3$) δ_H: 9.95 (s, 2H, CHO), 4.88 (t, J = 3.0 Hz, 4H, Fc), 4.67 (t, J = 3.0 Hz, 4H, Fc). ^{13}C NMR (400 MHz, $CDCl_3$) δ_C: 192.99 (CHO), 74.34,

71.02, 69.84; IR (cm^{-1}) υ 3101 (C-H), 2831 (C-H), 1655 (C=O); MS (ES) (*m/z*) calculated for $C_{12}H_{10}FeO_2$: 242.01 found: 242.01 [M^+].

1,1'-Ferrocenediacrylic acid diethyl ester, compound 3

Triethyl phosphonoacetate (3.32 mL, 16.7 mmol, 3 equiv.) was dissolved in anhydrous EtOH (10 mL) and NaH (0.892 g, 33.45 mmol, 90%, 6 equiv.) was added under argon atmosphere. The reaction mixture was stirred for 2 h. Compound **2** (1.35 g, 5.58 mmol, 1 equiv.) dissolved in anhydrous ethanol (10 mL) was added and left to stir for 23 h. The reaction mixture was quenched with water (15 mL), and the organic components were extracted with EtOAc (5 × 10 mL). The combined organic fractions were dried over anhydrous $MgSO_4$ and filtered. The solvent was removed *in-vacuo* and the crude product was purified *via* column chromatography (silica gel, 2:1 hexane:ethyl acetate) to yield the product as a deep red solid (51%, 1.082 g, 2.83 mmol, R_f 0.82); MP: 94–95 °C; ^{1}H NMR (300 MHz, $CDCl_3$) δ_H: 7.40 (d, *J* = 15.8 Hz, 2H, Fc-CH), 5.97 (d, *J* = 15.8 Hz, 2H, CHCO), 4.41 (dt, *J* = 21.5, 1.9 Hz, 8H, Fc), 4.22 (q, *J* = 7.1 Hz, 4H, OCH_2), 1.33 (t, *J* = 7.1 Hz, 6H, CH_3) ppm. ^{13}C NMR (400 MHz, $CDCl_3$) δ_C: 167.07 (C=O), 144.01, 116.38, 80.13, 72.45, 69.90, 60.40, 14.47; IR (cm^{-1}) υ 3081 (C-H), 2979 (C-H), 1715 (C=O), 1627 (C=O); MS (ES) (*m/z*) calculated for $C_{20}H_{22}FeO_4$: 382.10, found: 405.08 [$M+Na^+$].

1,1'-Ferrocenedipropanoic acid diethyl ester, compound 4

Compound **3** (1.06 g, 2.78 mmol, 1 equiv.) dissolved in EtOAc (20 mL) was added to $Pd(OH)_2$ (5% wt. on carbon, 500 mg). The reaction mixture was stirred under H_2 atmosphere (balloon pressure) at room temperature for 22 h. The reaction mixture was filtered through a short pad of Celite®. The solution was dried over anhydrous $MgSO_4$, filtered and concentrated *in vacuo* to yield the product as an orange oil (96%, 1.03 g, 2.66 mmol, R_f 0.49); ^{1}H NMR (300 MHz, $CDCl_3$) δ_H: 4.14 (q, *J* = 6.00 Hz, 4H, OCH_2), 4.01 (s, 8H, Fc), 2.65 – 2.68 (m, 4H, $FcCH_2$), 2.53 – 2.48 (m, 4H, CH_2CO), 1.26 (t, *J* = 6.00 Hz, 6H, CH_3); ^{13}C NMR (400 MHz, $CDCl_3$) δ_C: 173.28 (C=O), 87.73, 68.75, 68.33, 60.54, 36.04, 24.91, 14.39;

IR (cm^{-1}) υ 3087 (C-H), 2980 (C-H), 1729 (C=O); MS (ES) (*m/z*) calculated for $C_{20}H_{26}FeO_4$: 386.11 Found: 386.11 [M^+].

1,1'-Ferrocenedipropanol, compound 5

Compound **4** (1.05 g, 2.72 mmol, 1 equiv.) was dissolved in anhydrous THF (20 mL) and the reaction mixture was cooled to 0 °C for 15 min under argon atmosphere. Next, $LiAlH_4$ (1.0 M in THF, 10.7 mL, 10.64 mmol, 4 equiv.) was added dropwise and the reaction mixture was left to stir at 0 °C for 2 h. The reaction mixture was quenched with saturated aqueous sodium potassium tartrate solution (30 mL). The organic components were extracted with Et_2O (4 × 10 mL). The organic fractions were combined and dried over anhydrous $MgSO_4$ and filtered. The solvent was removed *in-vacuo* and the crude product was purified *via* column chromatography (silica gel, 1:1 ethyl acetate: hexane) to yield the product as an orange oil (87%, 0.720 g, 2.37 mmol, R_f 0.19); ^{1}H NMR (300 MHz, $CDCl_3$) δ_H: 4.00 (s, 8H, Fc), 3.67 (q, *J* = 5.74 Hz, 3H, CH_2OH), 2.42 (t, *J* = 5.84 Hz, 4H, FcC*H*$_2$), 1.77 (ddt, *J* = 9.5, 7.6, 6.4 Hz, 4H, FcCH$_2$C*H*$_2$), 1.28 (t, *J* = 5.4 Hz, 2H, CH$_2$O*H*); ^{13}C NMR (400 MHz, $CDCl_3$) δ_C: 89.72, 69.42, 68.65, 62.74, 34.17, 25.71; IR (cm^{-1}) υ 3307 (O-H), 2933 (C-H); MS (ES) (*m/z*) calculated for $C_{16}H_{22}FeO_2$: 302.10 found: 302.10 [M^+].

Compound 6 (Monotrityl protection of 1,1'-ferrocenedipropanol)

Compound **5** (500 mg, 1.66 mmol, 1 equiv.) was dissolved in anhydrous THF (20 mL) under an argon atmosphere. DMT–Cl (420 mg, 1.24 mmol, 0.75 equiv.), DIPEA (0.29 mL, 1.66 mmol, 1 equiv.) and DMAP (50 mg, 0.41 mmol, 4 equiv.) were added to the reaction mixture which was then left to stir at room temperature under argon atmosphere for 23 h. The reaction was quenched with saturated $NaHCO_3$ solution (20 mL) and the organic components were extracted with CH_2Cl_2 (3 × 20 mL). The combined organic fractions were dried over anhydrous Na_2SO_4 and filtered. The solvent was removed *in-vacuo* and product was purified *via* column chromatography (silica gel, 2:1 hexane:ethyl acetate, silica gel deactivated using 1% triethylamine) to yield the product as a yellow-orange oil (57%, 0.424 g, 0.7024 mmol, R_f 0.27); ^{1}H NMR (300 MHz, $CDCl_3$) δ_H: 7.42 – 7.08 (m, 9H, DMTr), 6.75 (d, *J* = 9.0 Hz, 4H,

DMTr), 3.93 – 3.82 (m, 8H, Fc), 3.70 (s, 6H, DMTr), 3.55 (t, *J* = 6.4 Hz, 2H, CH_2OH), 3.02 (t, *J* = 6.4 Hz, 2H, CH_2ODMTr), 2.32 (t, *J* = 8.4 Hz, 4H, $FcCH_2$), 1.80 – 1.61 (m, 4H, $FcCH_2CH_2$), 1.36 (s, 1H, CH_2OH); ^{13}C NMR (400 MHz, $CDCl_3$) δ_C: 158.40, 145.48, 136.76, 130.13, 128.29, 127.81, 126.70, 113.08, 89.01, 88.45, 85.83, 68.70, 68.65, 67.99, 67.86, 63.21, 62.69, 55.30, 34.28, 31.50, 26.09, 25.82; IR (cm^{-1}) *υ* 3367 (O-H), 2933 (C-H); MS (ES) (*m/z*) calculated for $C_{37}H_{40}FeO_4$: 604.22. Found: 605.23 $[M+H]^+$.

Compound 7 (Phosphitylation of Monotrityl ferrocene)

Compound **6** (191.3 mg, 0.32 mmol, 1 equiv.) was azeotroped with anhydrous dichloromethane (2 × 20 mL), then redissolved in anhydrous dichloromethane (10 mL) under argon. To the resulting solution was added DIPEA (0.14 mL, 0.79 mmol, 2.5 equiv.) followed by 2-cyanoethyl *N,N*–diisopropylchloeophosphoramidite (0.11 mL, 0.47 mmol, 1.5 equiv.). The reaction was left to stir for 2 h under argon. The reaction was then quenched with degassed ethyl acetate (20 mL) and the mixture was washed with degassed saturated aqueous $NaHCO_3$ (10 mL) and degassed brine (10 mL) and dried over anhydrous Na_2SO_4. This was then filtered and concentrated *in-vacuo* and the product was purified *via* column chromatography (silica gel, 1:1 hexane:ethyl acetate, silica gel deactivated using 1% triethylamine) to yield the product as an orange oil (70%, 178.2 mg, 0.2214 mmol, R_f 0.53); ^1H NMR (300 MHz, CD_3CN) δ_H: 7.39 – 7.14 (m, 9H, DMTr), 6.78 – 6.72 (m, 4H, DMTr), 3.90 – 3.82 (m, 8H, Fc), 3.76 – 3.67 (m, 8H, CH_2CH_2CN), 3.59 – 3.48 (m, 4H, CH_2OP, NCH), 3.01 (t, *J* = 6.4 Hz, 2H, CH_2ODMTr), 2.53 (t, *J* = 6.6 Hz, 2H, CH_2CN) 2.37 – 2.28 (m, 4H, $FcCH_2$), 1.79 – 1.68 (m, 4H, $FcCH_2CH_2$), 1.11 (dd, *J* = 6.8, 3.5 Hz, 12H, CH_3); ^{31}P NMR (300 MHz, CD_3CN) δ_P: 147.37; IR (cm^{-1}) *υ* 3084 (C-H), 2964 (C-H); MS (ES) (*m/z*) calculated for $C_{46}H_{57}FeN_2O_5P$: 804.79. Found: 805.76 $[M+H]^+$.

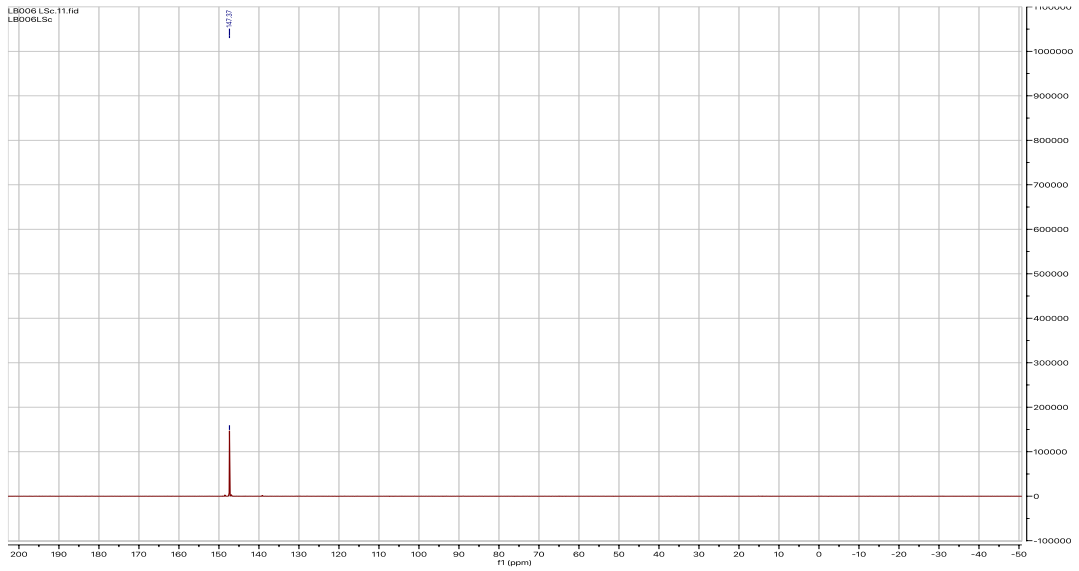

Figure S1: ^{31}P NMR spectrum of compound **7** in CD_3CN.

S2: Oligonucleotide Synthesis and Purification

S2.1 SYNTHESIS

Oligonucleotides were synthesised on an Applied Biosystems ABI 394 (Foster City, CA, 30 U.S.A). Standard phosphoramidites of Pac-dA, iPr-Pac-dG, Ac-dC, dT were purchased from Link Technologies and 3'-thiol-modifier 6 S-S CPG from Glen Research. The phosphoramidites (including compound **7**) were dissolved in anhydrous acetonitrile prior to synthesis (at 0.1 M). Strands were synthesised at a 1µmol scale on SynBase™ CPG 1000/110 solid supports from Link Technologies. Phosphoramidites were activated with 5-ethylthio-1H-tetrazole (0.25 M) in acetonitrile prior to coupling. Coupling times of 25 s were used for the nucleoside phosphoramidites, and 10 min for the ferrocene phosphoramidite moiety. Then, phenoxyacetic anhydride and methylimidazole were added to cap unreacted material, and iodine (0.02 M) in THF/pyridine/water (7:2:1) was added to oxidise the phosphotriester formed. Upon sequence completion, the resins were placed in freshly prepared 1 ml solutions of potassium carbonate (0.05 M) in methanol and left overnight to cleave strands from the resin and remove protecting groups. The solutions were neutralised with acetic acid (6 µl) and the solvent was removed on a Thermo

Scientific speed vac. The dried powders were redissolved in 1 ml Milli-Q water and desalted with a NAP-10 column (GE Healthcare) to remove residual resin and potassium carbonate. The solutions were then concentrated to 1 ml and stored in a freezer.

S2.2 Purification and Characterisation

Semi preparative HPLC purification was performed on an Agilent Technologies 1260 Infinity system using a Phenomenex Clarity 5 μm Oligo-RP LC 250 × 10 mm column. The column was heated to 60 °C prior to sample injection. The UV/vis absorbance of each run was monitored at 260 nm. The solvent gradient systems used are listed in Table S1 below:

Table S1. Eluent and Gradient Conditions for HPLC

Time	% TEAA 0.1 M in HPLC Water	% HPLC Grade Acetonitrile
0.00	85	15
30.00	75	25
30.01	0	100
40.00	0	100
40.01	85	15
45.00	85	15

Collected fractions were evaporated to dryness, diluted to 1 ml in Milli-Q water, and desalted using a NAP-10 column (GE Healthcare), whilst eluting to 1.5 ml. The purity of the oligonucleotides was determined by analytical HPLC using a Phenomenex Clarity 5 μm Oligo RP LC 250 × 4.6 mm column on an Agilent Technologies 1260 Infinity system. Solvent gradients used were identical to semi preparative HPLC. The UV/vis absorbance of each run was monitored at 260 nm.

Samples showing >95% purity by analytical HPLC were deemed sufficiently pure for use in experiments. Samples showing <95% purity were repurified by semi preparative HPLC. The characterisation of pure oligonucleotide samples was performed by negative mode electrospray mass spectrometry on a Waters Xevo G2-XS mass spectrometer. Sample concentrations were determined by optical density at 260 nm using a BioSpecnano micro-volume UV-Vis spectrophotometer (nanodrop)

from Shimadzu and the Beer Lambert law, with extinction coefficients obtained from Integrated DNA Technologies' OligoAnalyzer and a value of 3300 $M^{-1}cm^{-1}$ for the ferrocene moiety.

Table S2. DNA Strands and Characterisation Data

Name	Code	Description	Sequence	Predicted Mass / *m/z*	Detected Mass / *m/z*	Purity by analytical HPLC / %
2181	$ssDNA_{15}$	Fc-modified 15mer	5'-Fc TGG ACT CTC TCA ATG SSR-3'	5237.21	5237.06	100.00
2182	$ssDNA_{20}$	Fc-modified 20mer	5'-Fc TGG ACT CTC TCA ATG TGG AC SSR-3'	6801.47	6801.36	100.00
2183	$ssDNA_{25}$	Fc-modified 25mer	5'-Fc TGG ACT CTC TCA ATG TGG ACT CTC T SSR-3'	8290.70	8291.70	100.00
2184	$ssDNA_{30}$	Fc-modified 30mer	5'-Fc TGG ACT CTC TCA ATG TGG ACT CTC TCA ATG SSR-3'	9839.60	9839.99	100.00
2208	comp-DNA_{15}	15mer Complementary	5'-CAT TGA GAG AGT CCA-3'	4598.82	4598.69	96.21
2209	comp-DNA_{20}	20mer Complementary	5'-GTC CAC ATT GAG AGA GTC CA-3'	6123.07	6122.91	99.42
2210	comp-DNA_{25}	25mer Complementary	5'-AGA GAG TCC ACA TTG AGA GAG TCC A-3'	7720.35	7720.15	99.59
2211	comp-DNA_{30}	30mer Complementary	5'-CAT TGA GAG AGT CCA CAT TGA GAG AGT CCA-3'	9259.59	9259.30	99.03

SSR 3'-thiol modifier:

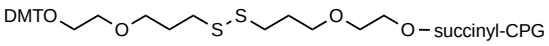

-SS-R'

S2.3 Analytical HPLC Traces

Strand 2181:

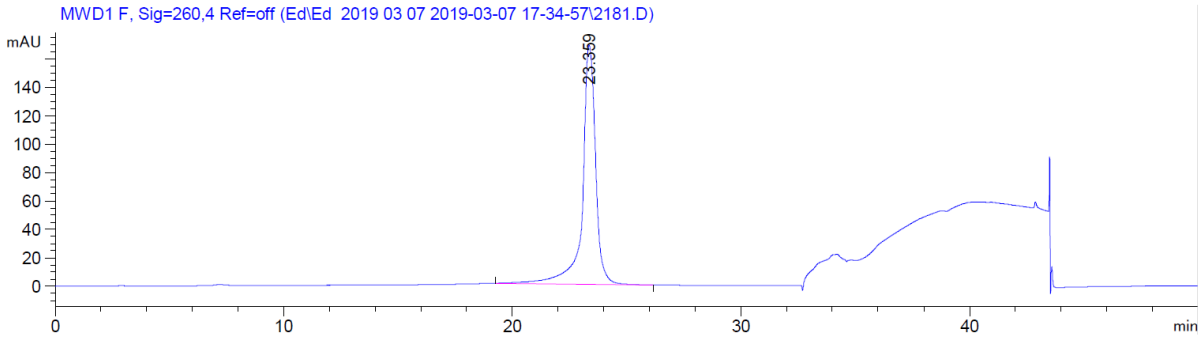

Signal 1: MWD1 F, Sig=260,4 Ref=off

Peak #	RetTime [min]	Type	Width [min]	Area [mAU*s]	Height [mAU]	Area %
1	23.359	BB	0.6121	6786.88916	168.43808	100.0000
Totals :				6786.88916	168.43808	

Strand 2182:

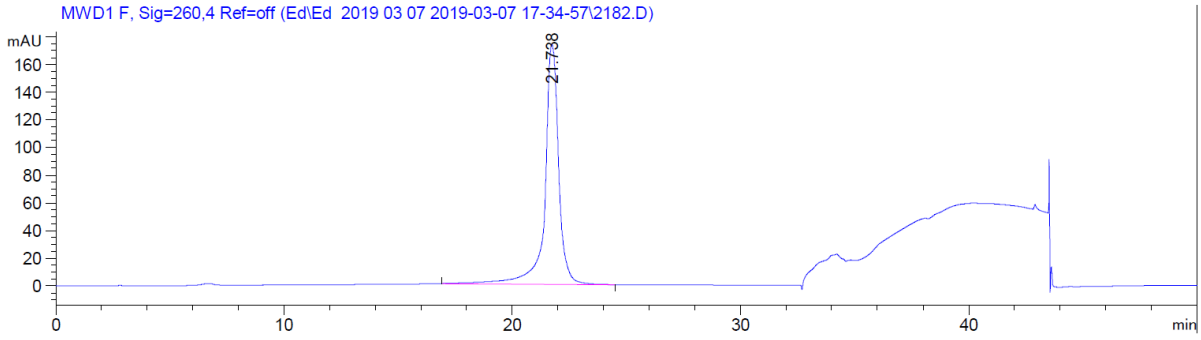

Signal 1: MWD1 F, Sig=260,4 Ref=off

Peak #	RetTime [min]	Type	Width [min]	Area [mAU*s]	Height [mAU]	Area %
1	21.738	BB	0.6342	7311.78076	173.29881	100.0000
Totals :				7311.78076	173.29881	

Strand 2183:

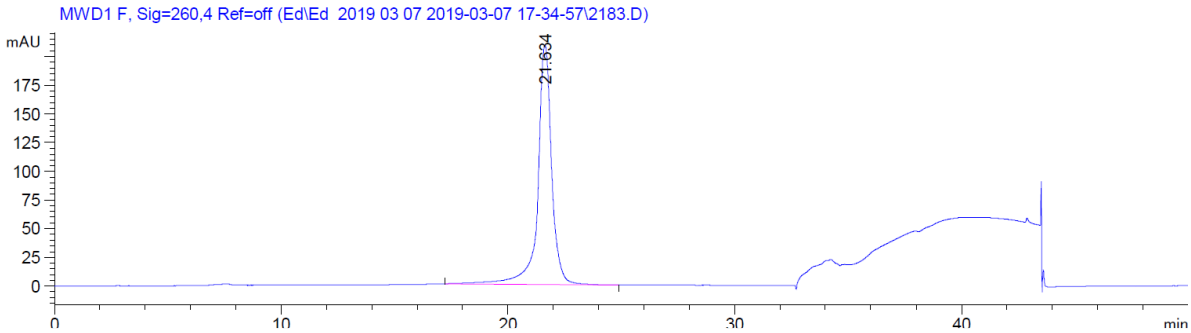

Signal 1: MWD1 F, Sig=260,4 Ref=off

Peak #	RetTime [min]	Type	Width [min]	Area [mAU*s]	Height [mAU]	Area %
1	21.634	BB	0.6387	8919.38477	208.65685	100.0000
Totals :				8919.38477	208.65685	

Strand 2184:

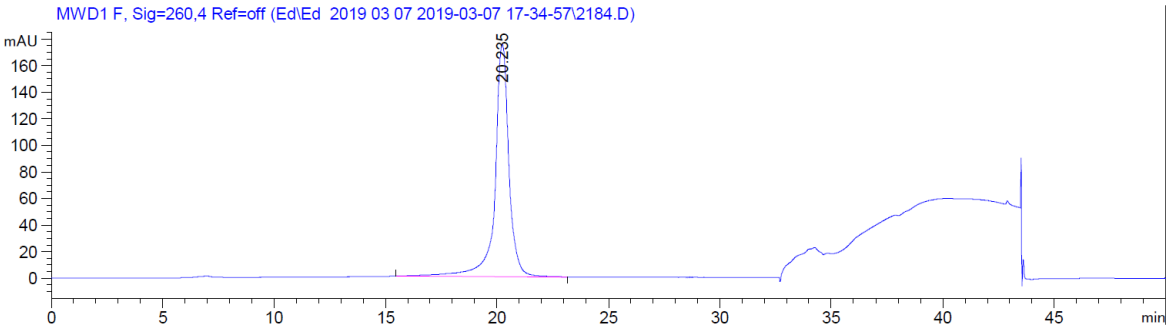

Signal 1: MWD1 F, Sig=260,4 Ref=off

Peak #	RetTime [min]	Type	Width [min]	Area [mAU*s]	Height [mAU]	Area %
1	20.235	BB	0.6514	7659.07227	174.73289	100.0000
Totals :				7659.07227	174.73289	

Strand 2208:

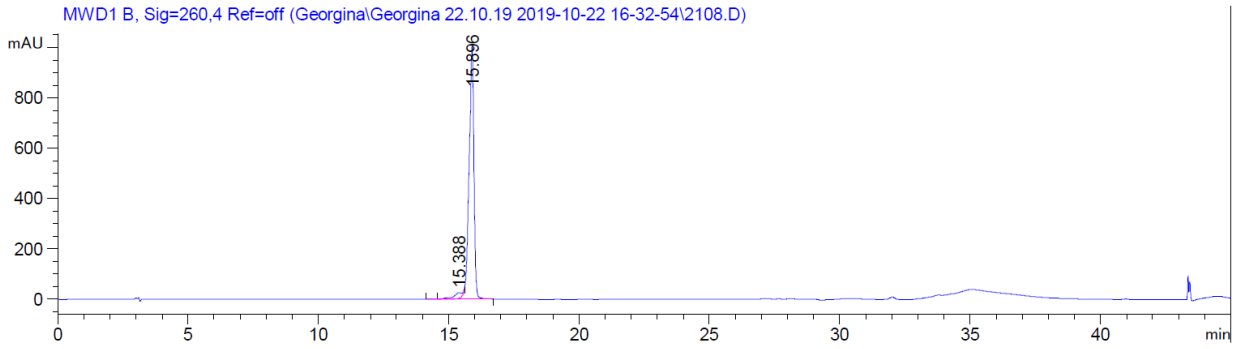

Signal 1: MWD1 B, Sig=260,4 Ref=off

Peak #	RetTime [min]	Type	Width [min]	Area [mAU*s]	Height [mAU]	Area %
1	15.388	VV E	0.2951	512.26184	23.43108	3.7944
2	15.896	VB R	0.1830	1.29883e4	1003.49646	96.2056
Totals :				1.35005e4	1026.92754	

Strand 2209:

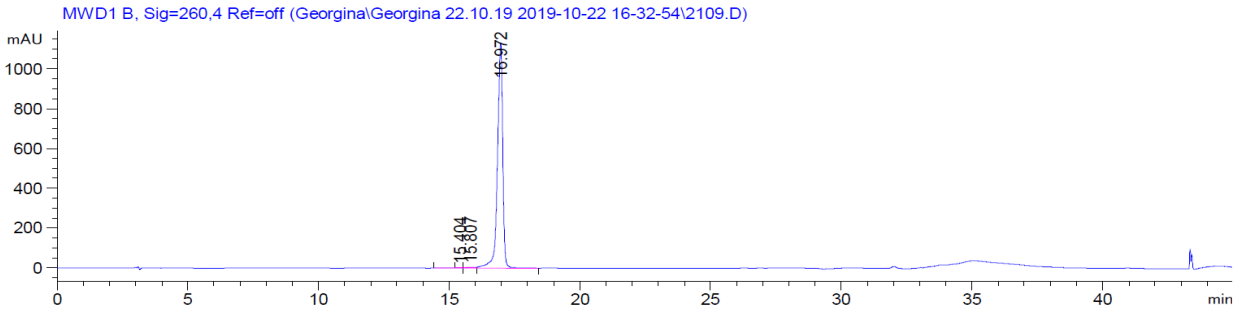

Signal 1: MWD1 B, Sig=260,4 Ref=off

Peak #	RetTime [min]	Type	Width [min]	Area [mAU*s]	Height [mAU]	Area %
1	15.404	VV E	0.2327	37.48465	2.22350	0.2344
2	15.807	VV E	0.2982	55.98345	2.43520	0.3501
3	16.972	VV R	0.1972	1.58953e4	1136.45984	99.4154
Totals :				1.59888e4	1141.11854	

Strand 2210:

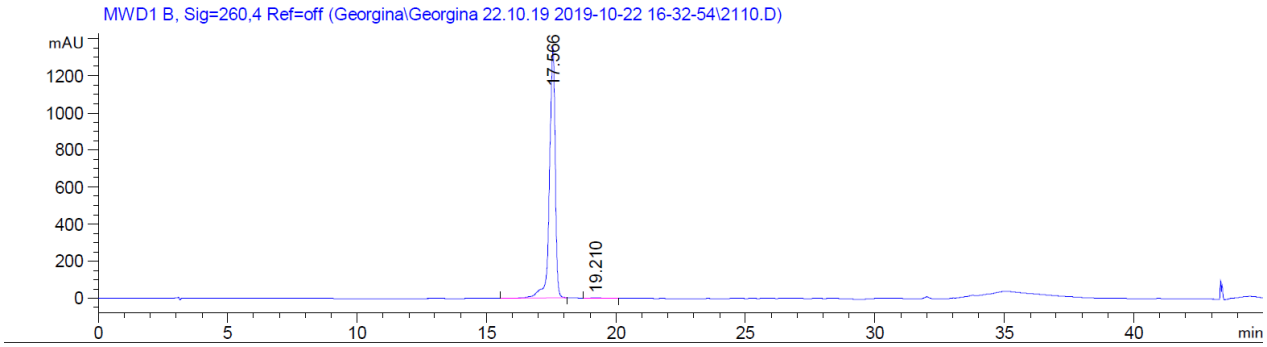

Signal 1: MWD1 B, Sig=260,4 Ref=off

Peak #	RetTime [min]	Type	Width [min]	Area [mAU*s]	Height [mAU]	Area %
1	17.566	VB R	0.2232	2.08417e4	1356.77820	99.5939
2	19.210	BB	0.4105	84.98764	2.69105	0.4061
Totals :				2.09267e4	1359.46925	

Strand 2211:

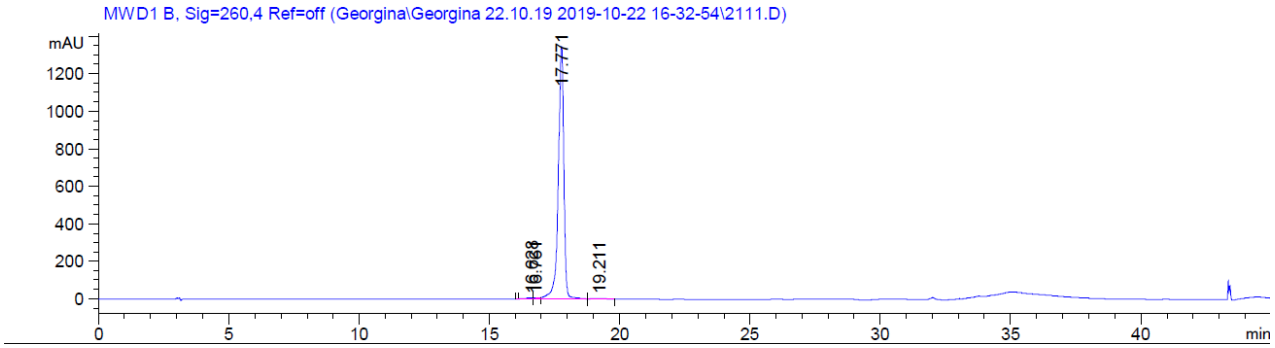

Signal 1: MWD1 B, Sig=260,4 Ref=off

Peak #	RetTime [min]	Type	Width [min]	Area [mAU*s]	Height [mAU]	Area %
1	16.628	BV E	0.2698	73.35106	3.56842	0.3624
2	16.761	VV E	0.1540	28.97577	2.68192	0.1432
3	17.771	VB R	0.2356	2.00442e4	1347.20972	99.0281
4	19.211	BB	0.3462	94.38791	3.37615	0.4663
Totals :				2.02409e4	1356.83621	

S2.4 Mass spectrometry data for Fc-modified strands

Strand 2181:

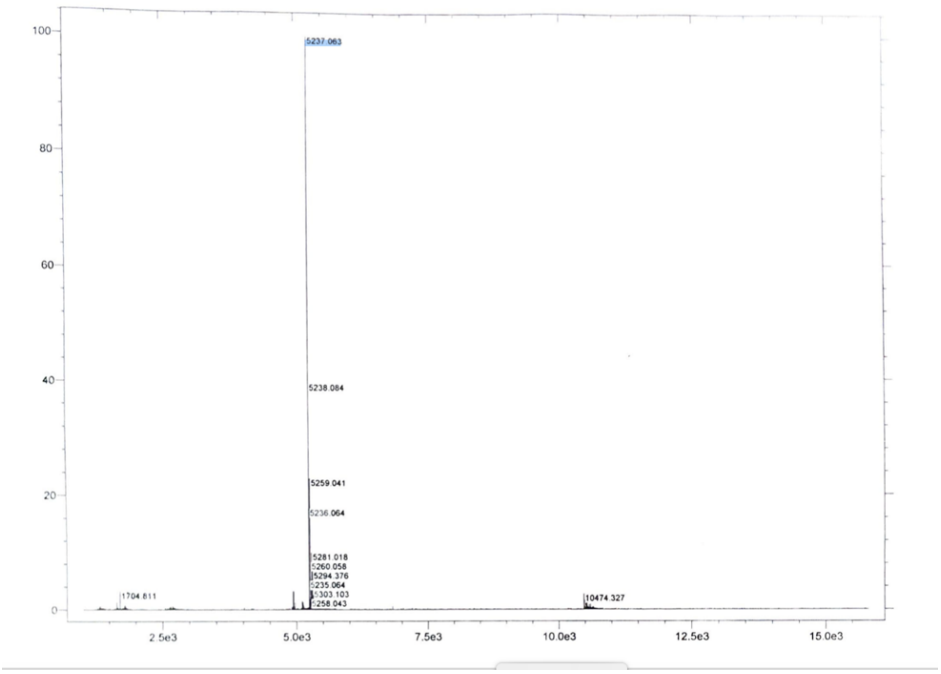

Figure S2: MS for 2181 Fc thiol

Strand 2182:

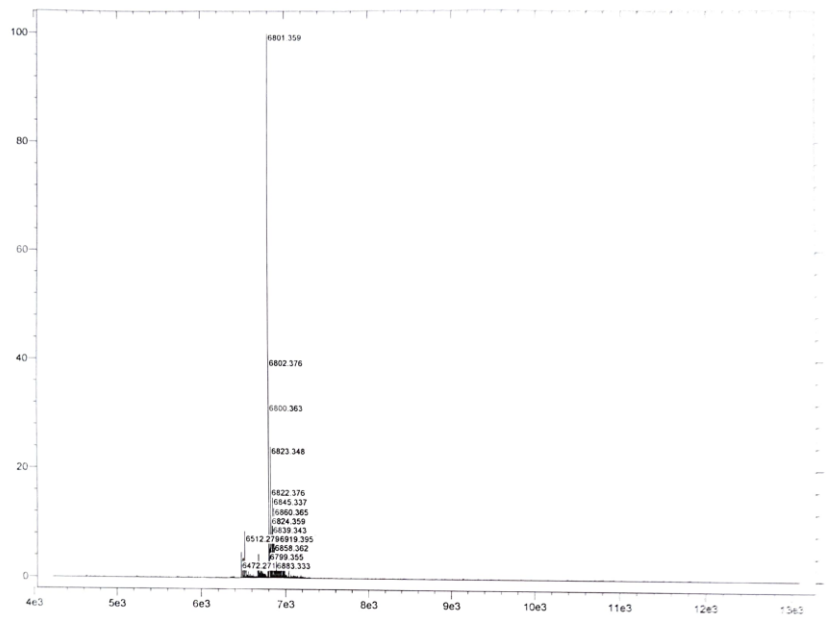

Figure S3: MS for 2182 Fc thiol

Strand 2183:

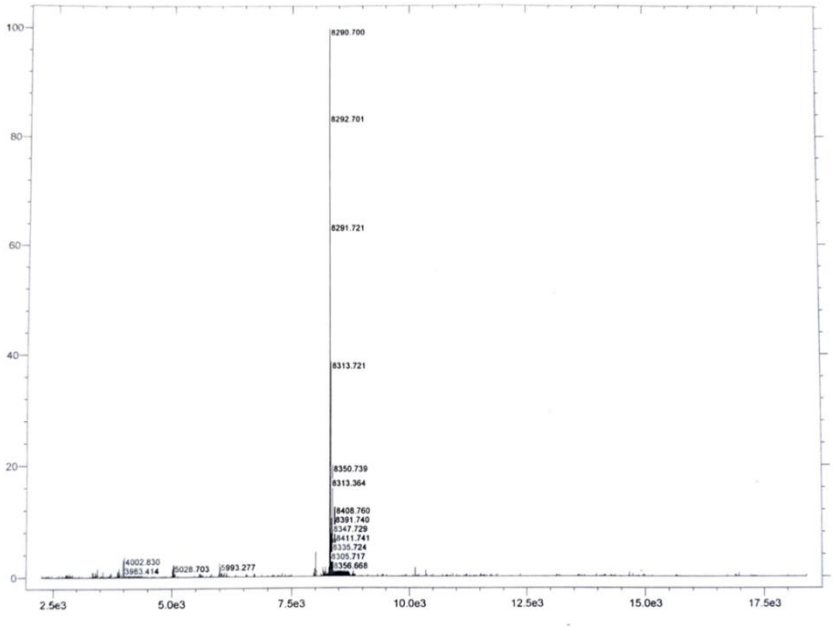

Figure S4: MS for 2183 Fc thiol

Strand 2184:

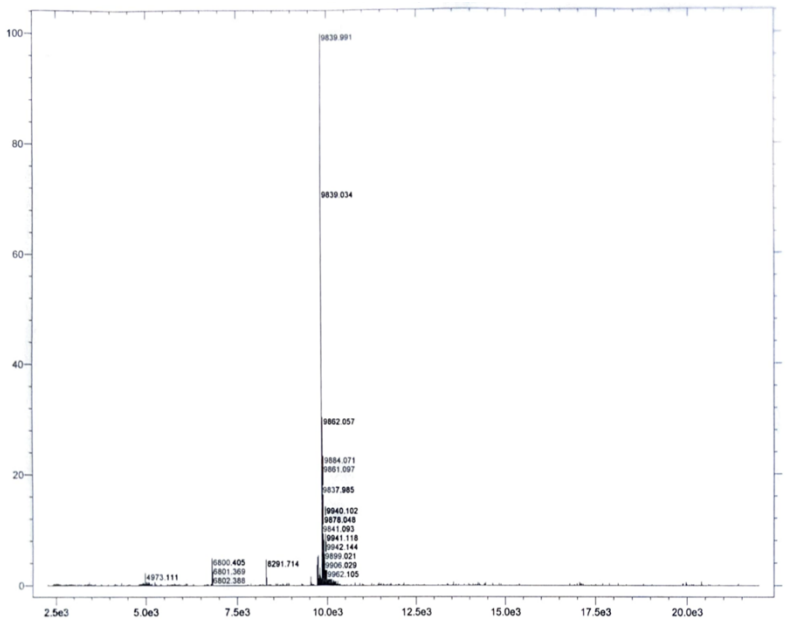

Figure S5: MS for 2184 Fc thiol

S3: SAM Formation and Charge Transport Studies

S3.1 Preparation of ssDNA and complementary DNA solutions

Each ssDNA sample was dissolved in 100 μL of pure deionised (DI) water to give a concentration of 50-100 μM. To cleave the disulphide bond and form the corresponding 3' thiol-terminated strand, 5 μL of the above-prepared 100 μL ssDNA solution was added to 5 μL of 10 mM TCEP in water. After a brief vortex to mix the two solutions, the Eppendorf tube was centrifuged to consolidate the solution at the bottom of the tube and was then left at 25 ºC for 60 min to reduce the disulphide bond. This solution was then diluted to 400 μL with 1 M NaClO4, 10 mM phosphate buffer, pH 7.0, (electrolyte) to give a final ssDNA concentration of ~ 1 μM.

The complementary DNA (comp-DNA) strand was dissolved in 300 μL of pure water and checked by UV/vis to have a concentration of 50-100 μM. This solution was then diluted six-fold, 150 μL plus 650 μL of electrolyte, to give an 800 μL solution (roughly 10 μM) ready for hybridisation with the ssDNA SAMs prefabricated on the Au substrates.

S3.2 Materials

We purchased gold (Au) and silicon wafers (100, p-type, 500 ± 25 μm) with one side polished from Super conductor Materials, inc. (USA) and University Wafers (USA), respectively. The polydimethylsiloxane (PDMS, Sylgard 184) was purchased from Sigma-Aldrich. The eutectic gallium-indium (EGaIn) alloy of 75.5 % Ga and 24.5 % In by weight was purchased from Sigma-Aldrich.

S3.3 PREPARATION OF TEMPLATE-STRIPPED AU

We used a previously reported method to prepare the ultra-smooth Au substrates.[2] Briefly, we evaporated 150 nm of Au at a rate of 0.5 Å/s by using a thermal evaporator at a base pressure of ~10^{-6} mbar. The evaporation rates for Au were ~0.3 Å/s. Glass slides were cleaned with piranha solution (30% H_2O_2: concentrated H_2SO_4 = 1:3) for 15 min, then rinsed thoroughly with deionised water and finally dried under a dinitrogen stream. These slides were then treated with plasma of oxygen for 5 min under 5 mbar. After that, we used a thermal adhesive (Epotek 353 ND) to glue the slides onto the Au surface followed by curing at 80°C in an oven for 3 hours.

S3.4 SAM GROWTH AND HYBRIDISATION

The ssDNA solution in the electrolyte was spread evenly on freshly template stripped Au with a micropipette and left undisturbed in a high moisture environment for 2 h. The substrates were rinsed with DI water and blow dried under a nitrogen stream prior to use. The Au substrates with ssDNA SAMs fabricated on them were placed in glass vials containing comp-DNA solutions and heated in a heating block pre-set at 70 °C for 10 minutes. The solutions with the substrates were then allowed to gently cool down to room temperature before they were rinsed with DI water and blown to dryness under a stream of nitrogen.

S3.5 SURFACE CHARACTERISATION OF THE SSDNA AND DSDNA SAMS WITH CV

The SAMs of Au-linker-DNA-Fc were electrochemically characterised by cyclic voltammetry. The electrochemical measurements were performed with an AUTOLAB PGSTAT302N instrument with NOVA 1.11 software. To perform cyclic voltammetry, we used a custom-built

electrochemical cell placed in a Faraday cage equipped with platinum wire as the counter electrode, an Ag/AgCl reference electrode and the Au electrode served as a working electrode. The cyclic voltammograms were recorded in an aqueous solution of the buffered solution of 10 mM NaH_2PO_4 and 1.0 M $NaClO_4$, between -0.2 to 1.0 V at a scan rate of 1.00 V/s. The surface coverage of the Fc units (Γ_{Fc}) was calculated using the total charge obtained by integration of the area under the anodic peak of the cyclic voltammogram (Q_{tot}), the number of electrons per mole of reaction (n), F is the Faraday constant (96485 C/mol), and A is the surface area of the electrode exposed to the electrolyte solution (0.5 cm^2) and is given by $\Gamma_{Fc} = Q_{tot}/nFA$. The electrochemical parameters for Fc terminated ssDNA and dsDNA SAMs on Au are the peak anodic potential (E_{pa}), peak cathodic potential (E_{pc}), peak separation ($\Delta E_p = | E_{pa} - E_{pc} |$), ratio of peak anodic and cathodic current (I_{pa}/I_{pc}), peak full-with at half maximum at anodic and cathodic peaks (FWHM E_{pa} and FWHM E_{pc}), the energy of the highest occupied molecular orbital (E_{HOMO}) and surface coverage of the ferrocene units (Γ_{Fc}).

Table S3: The electrochemical parameters for SC_nFc SAMs on Au surfaces obtained from averaging the values obtained from three independent experiments

DNA	Γ_{Fc} ($\times 10^{-10}$ mol/cm^2)	E_{pa} (mV)	E_{pc} (mV)	ΔE_p (mV)	I_{pa} / I_{pc}	FWHM E_{pa} (mV)	FWHM E_{pc} (mV)	E_{HOMO} (eV)
$ssDNA_{15}$	3.71 ± 0.17	431 ± 17	332 ± 6	99 ± 18	1.5 ± 0.1	315 ± 8	396 ± 3	-5.11 ± 0.02
$ssDNA_{20}$	3.95 ± 0.35	431 ± 2	347 ± 9	83 ± 9	2.0 ± 0.5	308 ± 6	483 ± 12	-5.12 ± 0.01
$ssDNA_{25}$	3.09 ± 0.56	393 ± 12	323 ± 15	69 ± 20	1.2 ± 0.4	299 ± 25	253 ± 36	-5.07 ± 0.02
$ssDNA_{30}$	3.28 ± 0.38	406 ± 13	329 ± 15	77 ± 20	1.1 ± 0.3	299 ± 6	316 ± 64	-5.09 ± 0.02
$dsDNA_{15}$	2.23 ± 0.32	424 ± 9	354 ± 25	70 ± 27	0.9 ± 0.3	329 ± 44	284 ± 9	-5.12 ± 0.03
$dsDNA_{20}$	2.29 ± 0.57	468 ± 12	374 ± 7	95 ± 14	0.9 ± 0.3	340 ± 31	330 ± 22	-5.17 ± 0.02
$dsDNA_{25}$	2.83 ± 0.35	395 ± 12	321 ± 9	73 ± 15	1.2 ± 0.1	354 ± 36	281 ± 24	-5.07 ± 0.02
$dsDNA_{30}$	2.32 ± 0.44	429 ± 25	354 ± 9	75 ± 27	1.6 ± 0.6	282 ± 12	345 ± 54	-5.13 ± 0.02

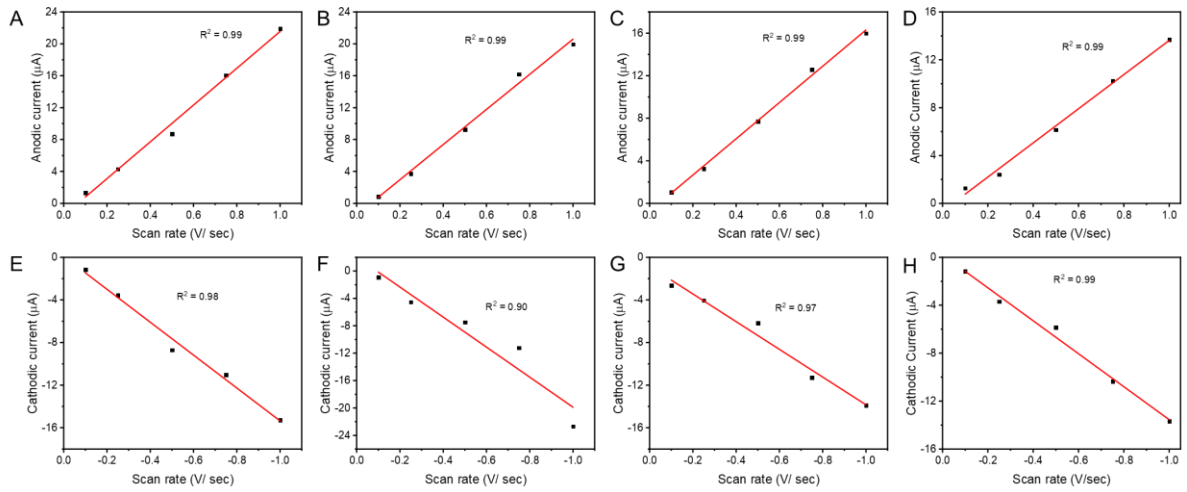

Figure S6: Scan rate as a function of the anodic peak current for (A) $ssDNA_{15}$, (B) $ssDNA_{20}$, (C) $ssDNA_{25}$ and (D) $ssDNA_{30}$; and the scan rate as a function of the cathodic peak current (E) $ssDNA_{15}$, (F) $ssDNA_{20}$, (G) $ssDNA_{25}$ and (H) $ssDNA_{30}$ SAMs

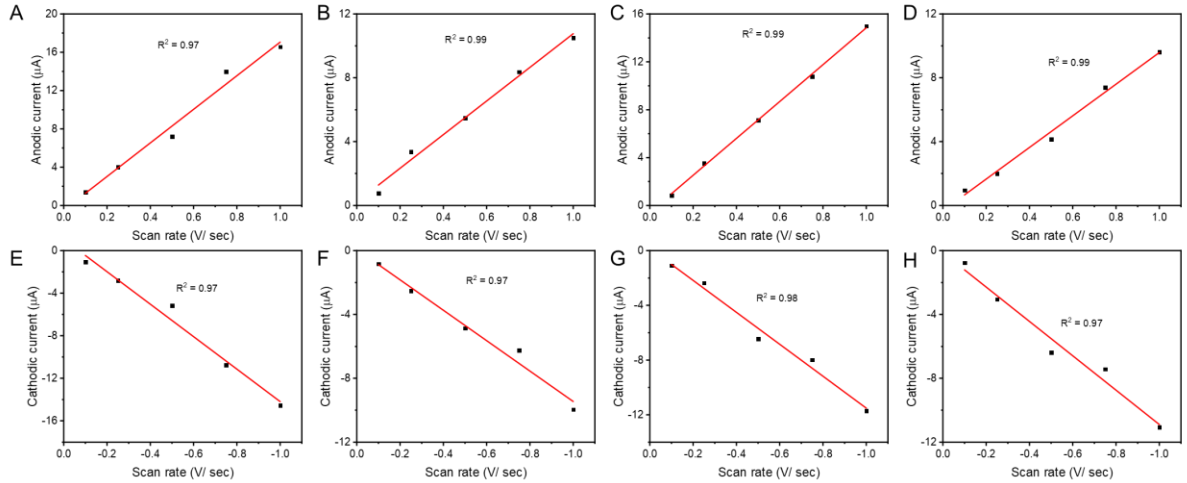

Figure S7: Scan rate as a function of the anodic peak current for (A) $dsDNA_{15}$, (B) $dsDNA_{20}$, (C) $dsDNA_{25}$ and (D) $dsDNA_{30}$; and the scan rate as a function of the cathodic peak current (E) $dsDNA_{15}$, (F) $dsDNA_{20}$, (G) $dsDNA_{25}$ and (H) $dsDNA_{30}$ SAMs

S3.6 SURFACE CHARACTERISATION WITH AR-XPS, NEXAFS AND UPS

Angle-resolved AR-XPS was performed at the soft X-ray spectroscopy beamline of the Australian Synchrotron. The samples were placed in an ultra-high vacuum chamber with a base pressure of ~10^{-10} mbar at room temperature. The Au $4f_{7/2}$ peak (~84.0 eV) of a sputter-cleaned gold foil inside the chamber was used to calibrate the photon energy before measuring each sample. Survey scans (photon energy = 850 eV) were used to determine the region of interest before high resolution scans were recorded for each element. To enhance the photoionisation cross section and surface sensitivity of XPS, we used incident photon energy 650 eV for O 1*s* and N 1*s*, and 350 eV for S 2*p*, C 1*s*, Au 4*f* and P 2*p* to record the spectra. We recorded the XPS signals at two different take-off angles for photoelectrons: 90° (normal emission, NE) and 40° (grazing emission, GE). The peak fitting was performed with a pseudo-Voigt function using a fixed 70% Gaussian and 30% Lorentzian functions.

Peak assignment for Au 4*f*, C 1*s*, N 1*s*, O 1*s* and P 2*p* are reported in Vilar *et al.* and S 2p has been reported by us previously.[3,4]

Table S4: Peak assignment for Au 4f, C 1s, N 1s, O 1s and P 2p

S. No.	Element	Peak	Assignment
1	Au	4f	Peak 1 84.0 eV; Au metal
2	C	1s	Peak 1: 284.8 eV; -C-C-, -C=, -CH Peak 2: 286.4; -C-N, N-C=N, C-O-C, -CH_2O- Peak 3: 288.0 eV; -C-NH_2, N-(CO)-C, N-CO-C
3	O	1s	Peak 1: 530.3 eV; C-O-C; N-(CO)-C Peak 2:531.9 eV; PO_4^-
4	S	2p	Peak S_1: 162.0 eV; chemisorbed S Peak S_2: 163.4; physiosorbed S
5	N	1s	Peak 1: 398.6 eV; -N= Peak 2: 400.0 eV; -NH_2, >N-; N-(CO)-N
6	P	2p	Peak 1: 133.4; PO_4^- Peak 2: 134.2; PO_4^-

Error: ±0 .1 eV

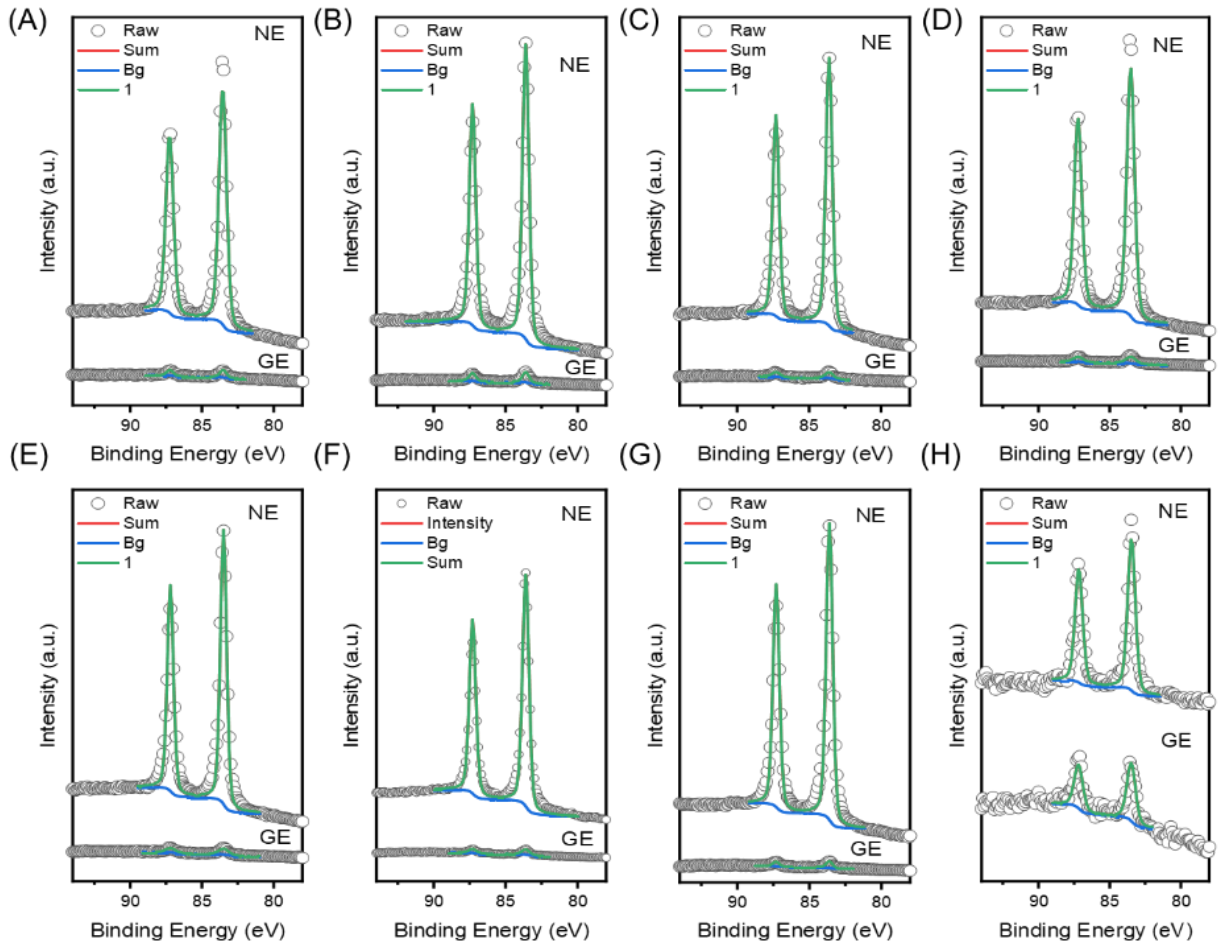

Figure S8: Au 4f spectra for (A) ssDNA$_{15}$, (B) ssDNA$_{20}$, (C) ssDNA$_{25}$ and (D) ssDNA$_{30}$; and (E) dsDNA$_{15}$, (F) dsDNA$_{20}$, (G) dsDNA$_{25}$ and (H) dsDNA$_{30}$ SAMs

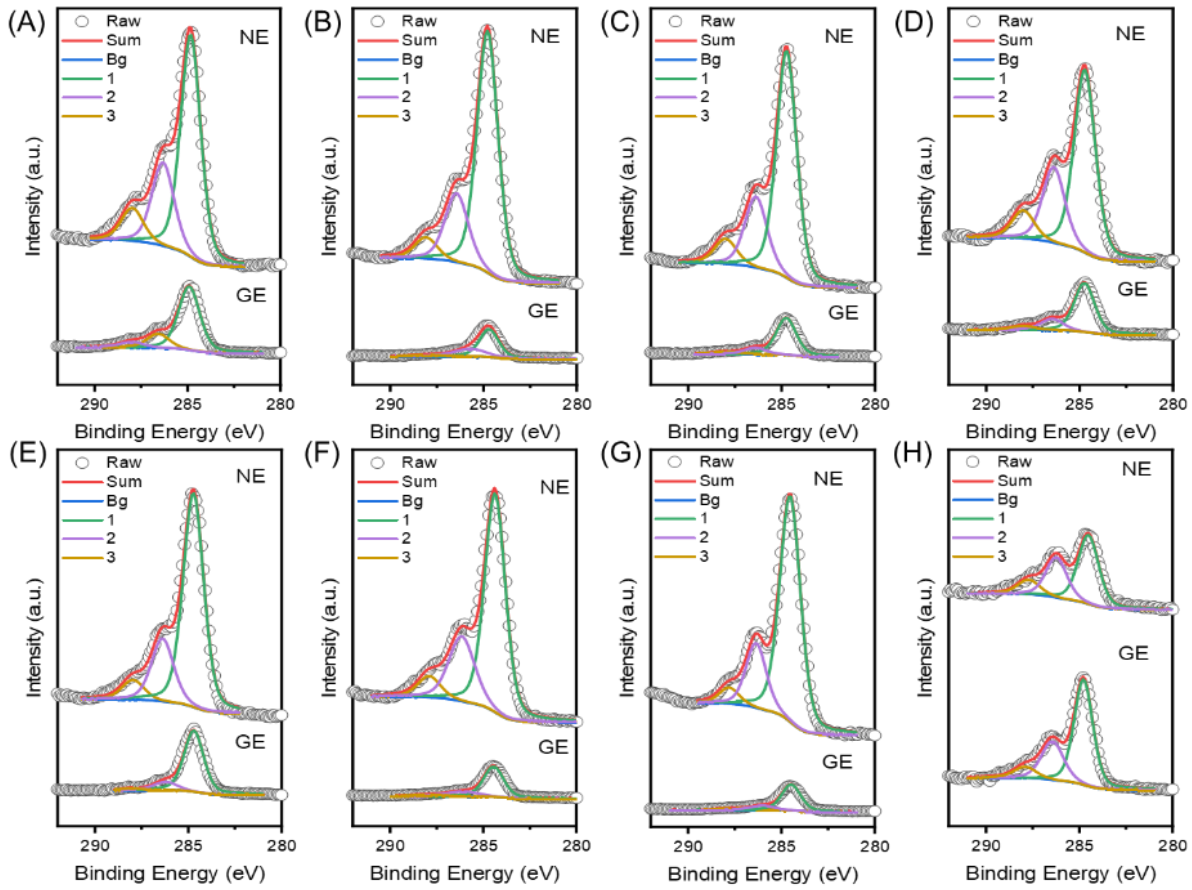

Figure S9: C 1s spectra for (A) ssDNA$_{15}$, (B) ssDNA$_{20}$, (C) ssDNA$_{25}$ and (D) ssDNA$_{30}$; and (E) dsDNA$_{15}$, (F) dsDNA$_{20}$, (G) dsDNA$_{25}$ and (H) dsDNA$_{30}$ SAMs

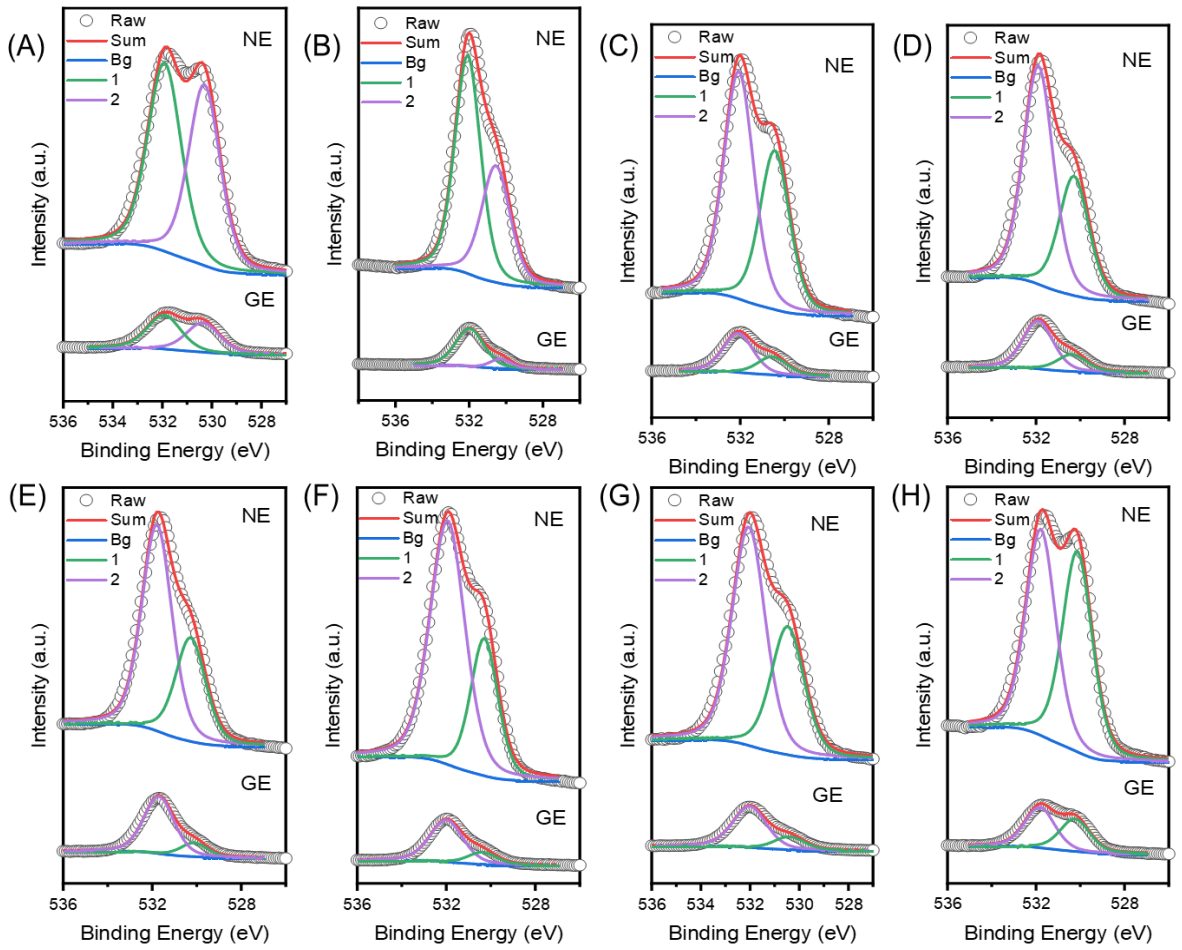

Figure S10: O 1s spectra for (A) ssDNA$_{15}$, (B) ssDNA$_{20}$, (C) ssDNA$_{25}$ and (D) ssDNA$_{30}$; and (E) dsDNA$_{15}$, (F) dsDNA$_{20}$, (G) dsDNA$_{25}$ and (H) dsDNA$_{30}$ SAMs

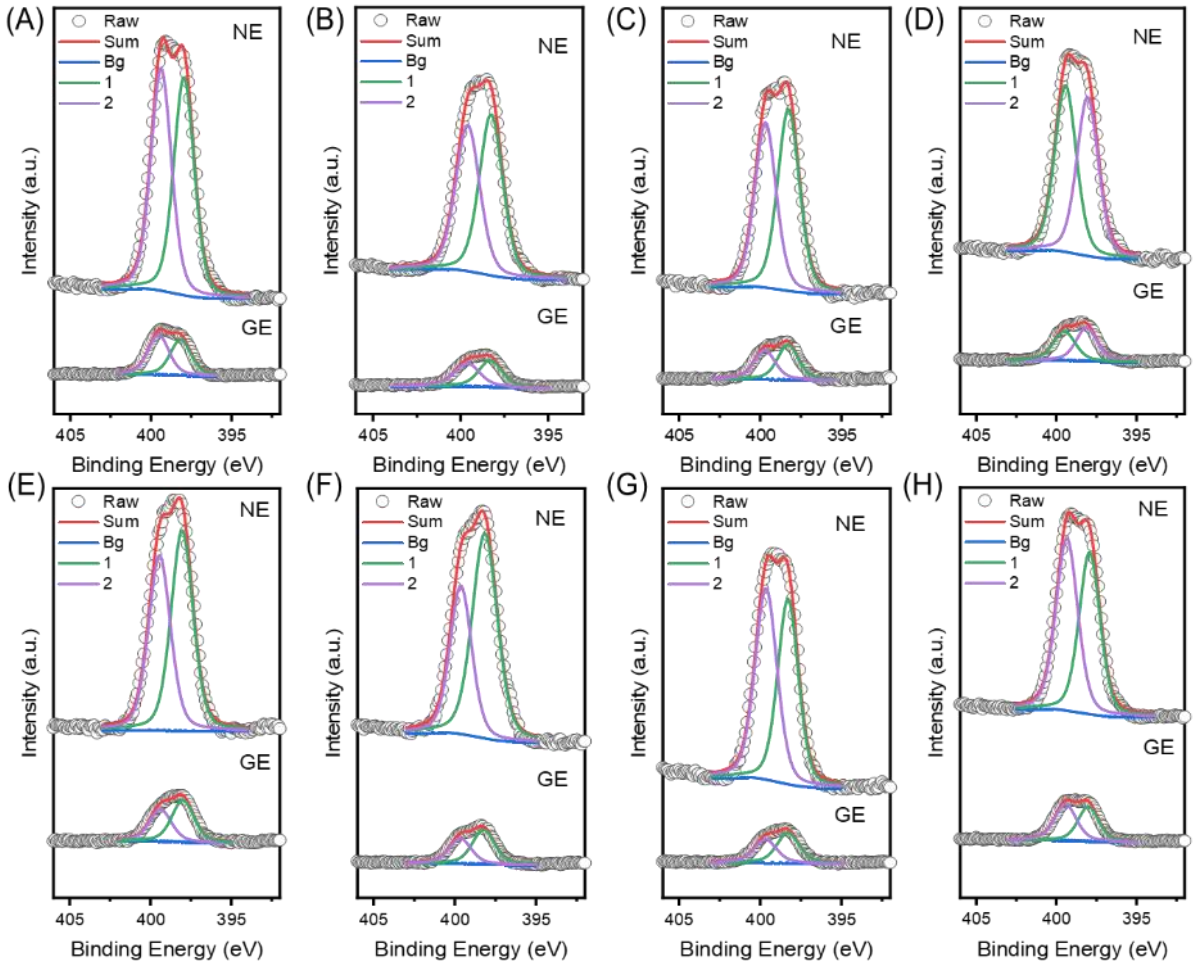

Figure S11: N 1s spectra for (A) ssDNA$_{15}$, (B) ssDNA$_{20}$, (C) ssDNA$_{25}$ and (D) ssDNA$_{30}$; and (E) dsDNA$_{15}$, (F) dsDNA$_{20}$, (G) dsDNA$_{25}$ and (H) dsDNA$_{30}$ SAMs

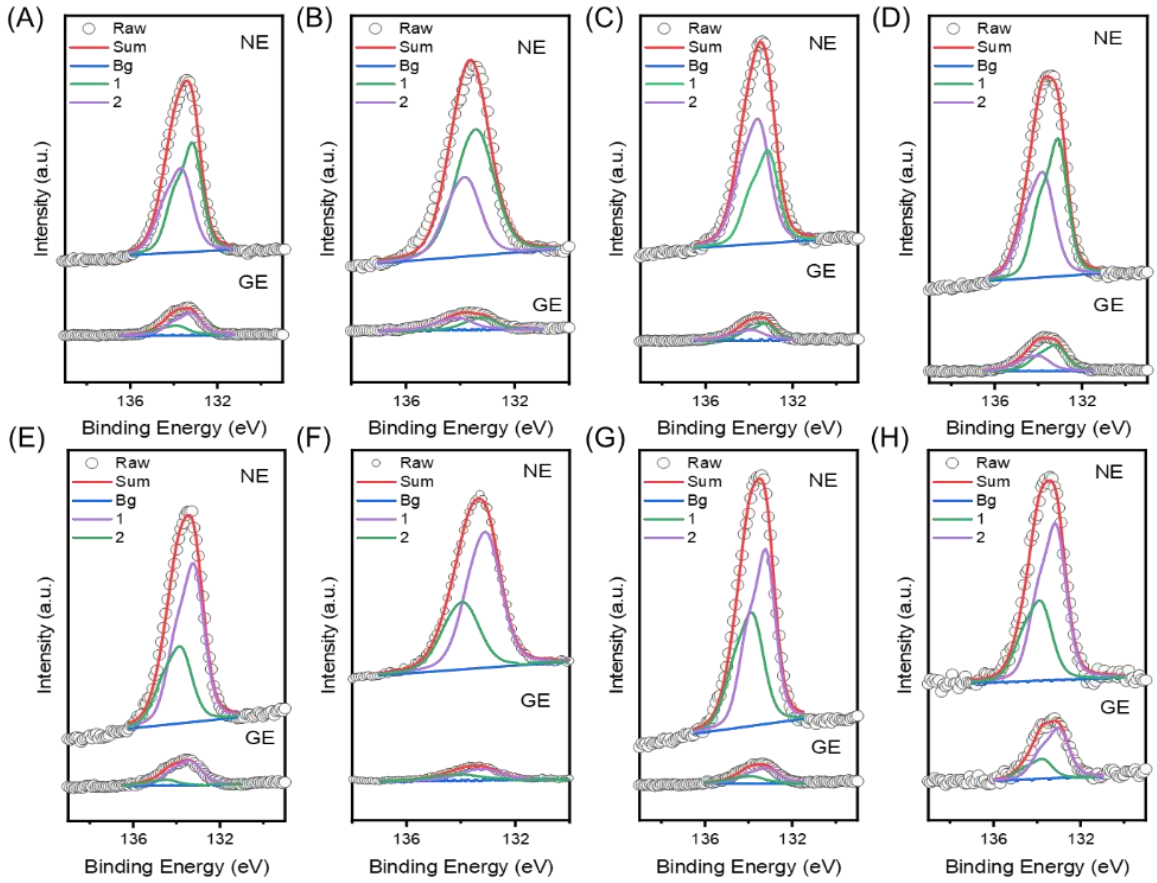

Figure S12: P 2p spectra for (A) ssDNA$_{15}$, (B) ssDNA$_{20}$, (C) ssDNA$_{25}$ and (D) ssDNA$_{30}$; and (E) dsDNA$_{15}$, (F) dsDNA$_{20}$, (G) dsDNA$_{25}$ and (H) dsDNA$_{30}$ SAMs

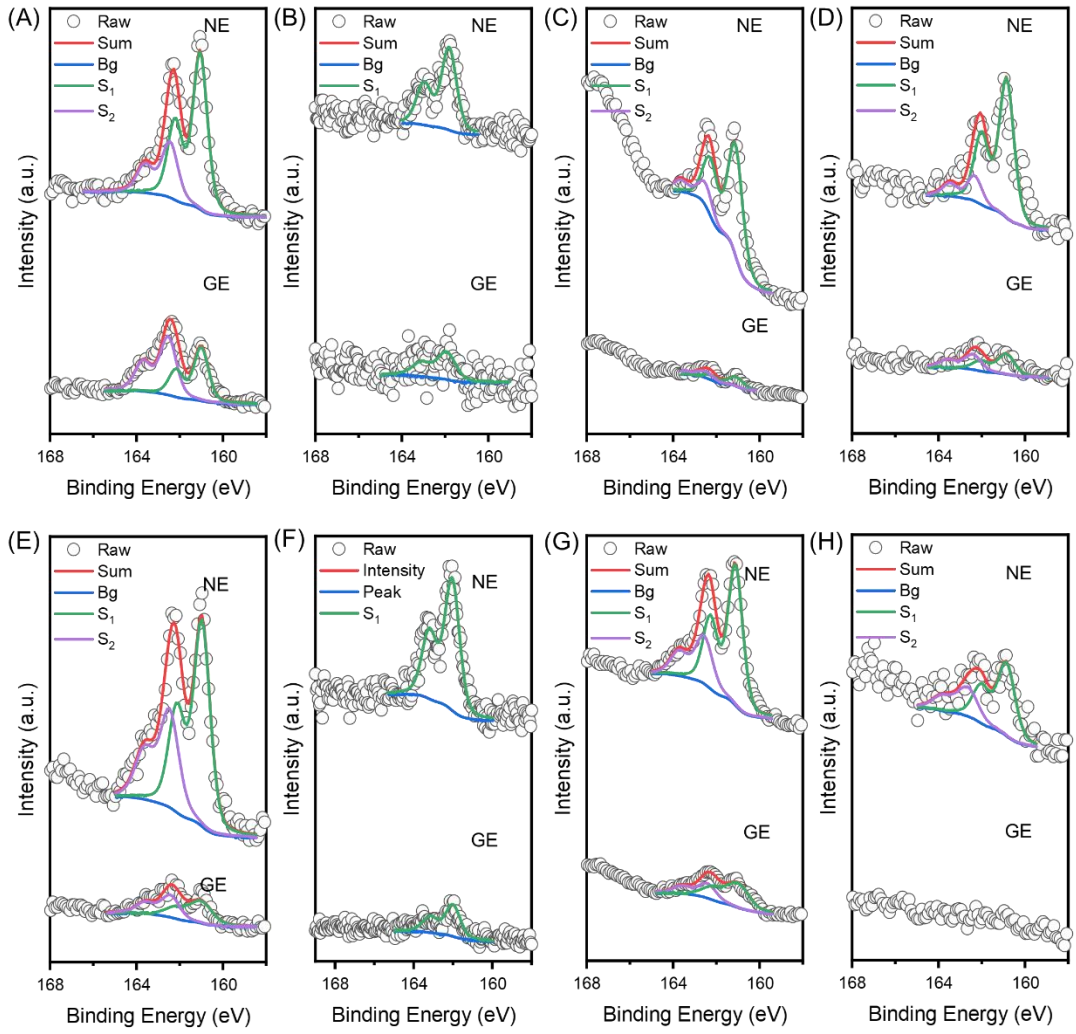

Figure S13: S 2p spectra for (A) ssDNA$_{15}$, (B) ssDNA$_{20}$, (C) ssDNA$_{25}$ and (D) ssDNA$_{30}$; and (E) dsDNA$_{15}$, (F) dsDNA$_{20}$, (G) dsDNA$_{25}$ and (H) dsDNA$_{30}$ SAMs

S3.7 DNA MONOLAYER THICKNESS BY ELLIPSOMETRY

The monolayer of ssDNA and dsDNA on Au surface as a function of base pair length were carried out by variable angle spectroscopic ellipsometry. We measured the amplitude ratio (Ψ) and change in phase (Δ) at a fixed wavelength (500 nm) as a function of the incident angle from 40° to 65° followed by fitting of the data to the Cauchy model, the real and imaginary parts of the refractive indices were taken from literature.[5–8] The data were fitted with Accurion Nanofilm_ep4 Ellipsometer software. Before the SAM formation, the refractive index (n) and

extinction coefficients (k) of the bare template stripped Au substrates were found by measuring the polarisation angles at three spots on each substrate. We measured angle incident angle dependent Ψ and Δ values and fit them with regression analysis to a three-layer model comprised of the glass support layer, Au and a Cauchy layer as the DNA monolayer with EP4Model software. The refractive index of the DNA was fixed according to the values that have been reported previously in the range of $n \in (1.3 – 1.4)$ and $k \in (0 – 0.2)$.[5,6]

S3.8 DATA COLLECTION OF $J(V)$ MEASUREMENTS AND THE EGAIN TECHNIQUE

Fabrication of the junctions was performed using reported procedures which are described elsewhere in detail.[9] The Au metal surface with SAMs was grounded and an external bias was applied to the top electrode. For the top electrode, we utilised a cone-shaped tip of EGaIn, where "//" refers to a van der Waals contact, "/" refers to the contact between EGaIn and GaO_x and "-" refers to a chemical contact. A Keithley 6340 source meter was utilised to apply an external bias with LabView 2010 to collect the $J(V)$ data. The bias was changed from 0 V→ 1 V → 0 V → -1 V → 0 V. 3 scans were recorded for each junction to check for junction stability and these scans were not included in analysis. Then, we recorded 20 traces which were used in our analysis before we formed a new junction. A summary of the $J(V)$ data and junction yields are shown in Table 2.

We followed the procedure for statistical analysis of the junction data as reported before.[9] Open circuits and shorts were not used for data analysis. The $\log_{10}|J|$ at each measured bias were plotted in a histogram, as shown in Fig. S9 and S10, and a normal distribution was utilised to obtain the Gaussian log-average value of $|J|$, the Gaussian log-standard deviation of J, σ_{log} and the 95% confidence bands. The histograms at ±1.0 V are shown in Fig. S3 and S4, for ssDNA and ds DNA, respectively. The $\log_{10}|J|$, σ_{log} values are shown in Table 2. The rectification ratio (R = (<log $|J|$> at +1.0 V)/ (<log $|J|$> at -1.0 V) is plotted in Fig. S11.

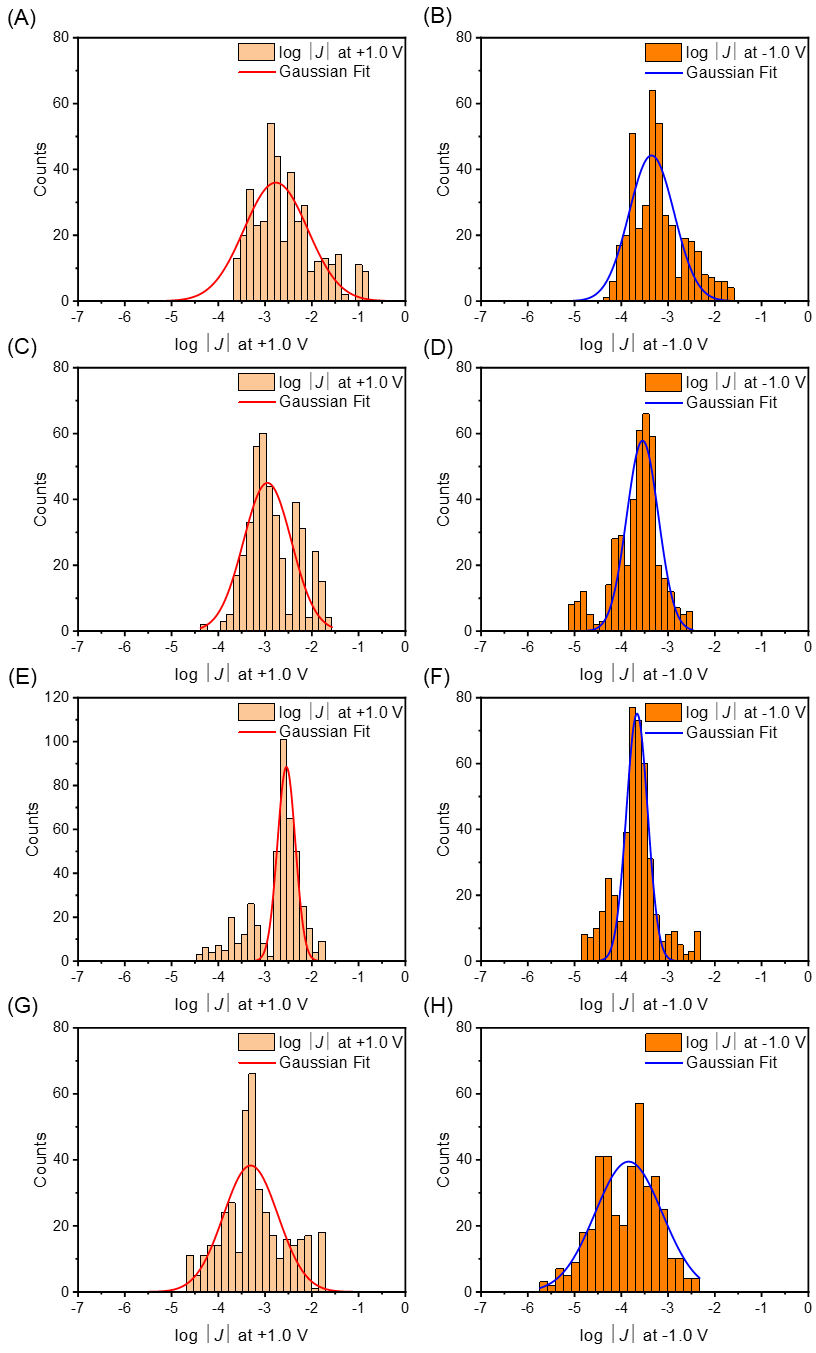

Figure S14: Histograms of log(|*J*|) obtained from Au/ssDNA//GaO_x/EGaIn junctions measured at +1.0 for (A) $ssDNA_{15}$, (C) $ssDNA_{20}$, (E) $ssDNA_{25}$ and (G) $ssDNA_{30}$ and at -1.0 V for (B) $ssDNA_{15}$, (D) $ssDNA_{20}$, (F) $ssDNA_{25}$ and (H) $ssDNA_{30}$.

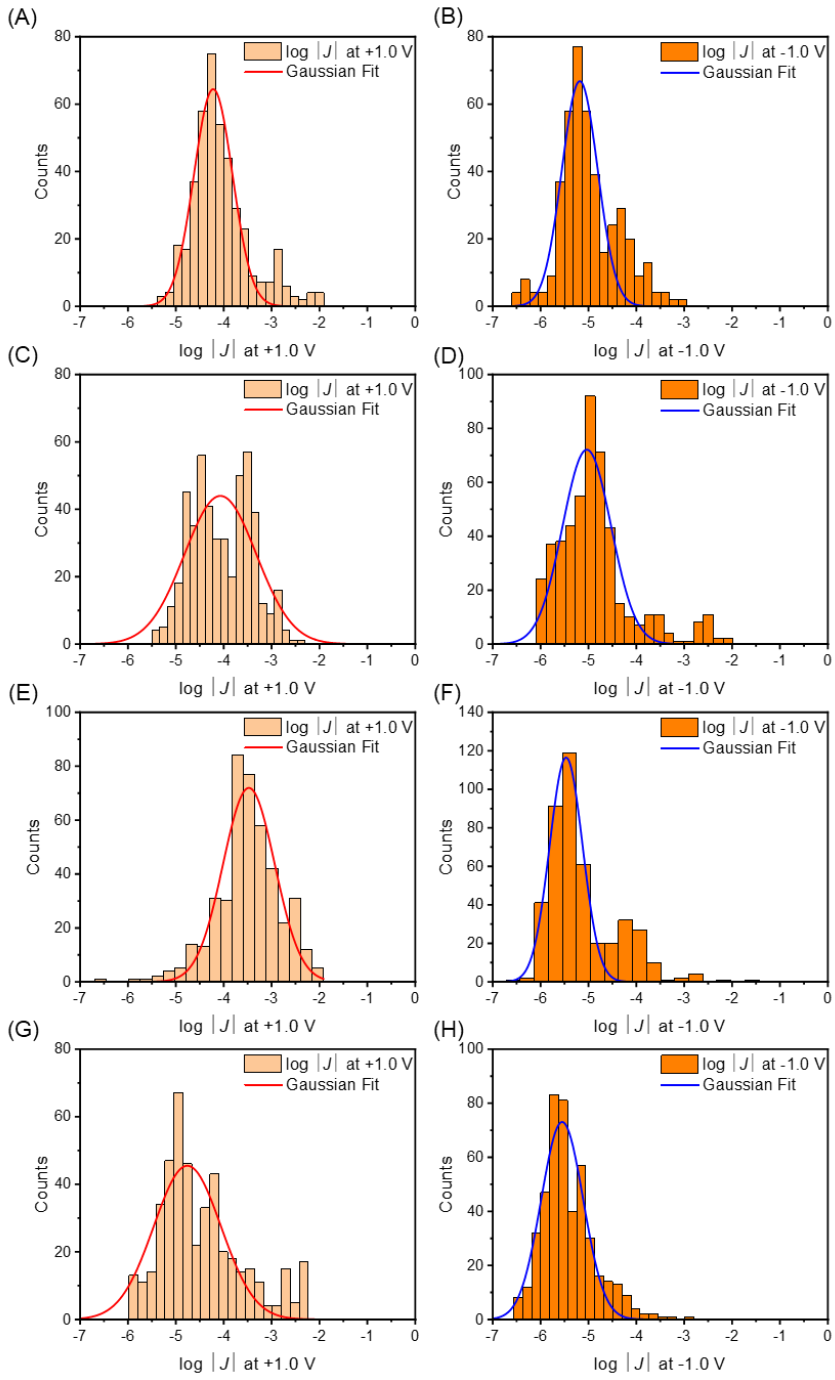

Figure S15: Histograms of log(|*J*|) obtained from Au/dsDNA//GaO_x/EGaIn junctions measured at +1.0 for (A) $dsDNA_{15}$, (C) $dsDNA_{20}$, (E) $dsDNA_{25}$ and (G) $dsDNA_{30}$ and at -1.0 V for (B) $dsDNA_{15}$, (D) $dsDNA_{20}$, (F) $dsDNA_{25}$ and (H) $dsDNA_{30}$.

Table S5: Summary of junction characteristics for ssDNA and dsDNA, errors presented are σ_{log}

Molecule	log |*J*| at -1.0 V (A/cm^2)	log |*J*| at +1.0 V (A/cm^2)	Total junctions	Stable junctions	Yield (%)
$ssDNA_{15}$	-5.22 ± 0.31	-4.21 ± 0.42	27	22	81.48
$ssDNA_{20}$	-5.05 ± 0.51	-4.08 ± 0.74	31	25	80.65
$ssDNA_{25}$	-5.28 ± 0.41	-3.69 ± 0.29	24	20	83.34
$ssDNA_{30}$	-5.55 ± 0.42	-4.75 ± 0.70	32	26	81.25
$dsDNA_{15}$	-3.35 ± 0.49	-2.75 ± 0.65	27	21	77.78
$dsDNA_{20}$	-3.55 ± 0.34	-2.96 ± 0.49	30	23	76.67
$dsDNA_{25}$	-3.67 ± 0.23	-2.54 ± 0.19	32	24	75.00
$dsDNA_{30}$	-3.85 ± 0.54	-3.32 ± 0.70	25	21	84.00

S3.9 TEMPERATURE DEPENDENT *J*(*V*) MEASUREMENTS

S3.9 TEMPERATURE DEPENDENT *J*(*V*) MEASUREMENTS

Measurements of *J*(V) as a function of temperature *T* (K) were carried out in a cryogenic probe station (Lakeshore CRX-VF) at a pressure of 1.0×10^{-5} bar. For fabrication of the Au bottom electrodes, we used e-beam evaporation processes to form arrays of 100 nm thick Au electrodes (10 μm wide and 5000 μm long, with 500 × 500 μm^2 square pads at their ends that facilitated addressing the electrodes with probes) on Si/SiO_2 wafers following previously reported methods.[10] Glass substrates, washed with piranha solution, ethanol and acetone and dried in an oven, were cut with a diamond scriber. Optical adhesive (OA, Norland, No. 61) was utilised to glue the glass substrates to the Au by curing under a UV lamp for 2 h. For preparation of the top contact stabilised in a PDMS (Sylgard 184) microchannel, A hole of 1.5 mm in diameter was punched a the entrance of the microchannel and a drop of EGaIn was placed on the hole. The PDMS microchannel was aligned on patterned Au electrodes and the PDMS channel with the Au electrodes was placed in a vacuum chamber 30 min (10^{-2} mbar). The channels filled spontaneously upon release of vacuum. Then, the device was placed in a probe station and degassed with nitrogen for 3 min to expel all air in the chamber. To prevent the EGaIn from

evacuating the microchannel upon application of vacuum, the probe station was cooled down to 240 K to freeze the EGaIn and then vacuum was applied. The substrates were subsequently cooled down to 150 K and measurements were conducted in the heat-up cycle with solid-EGaIn electrodes.

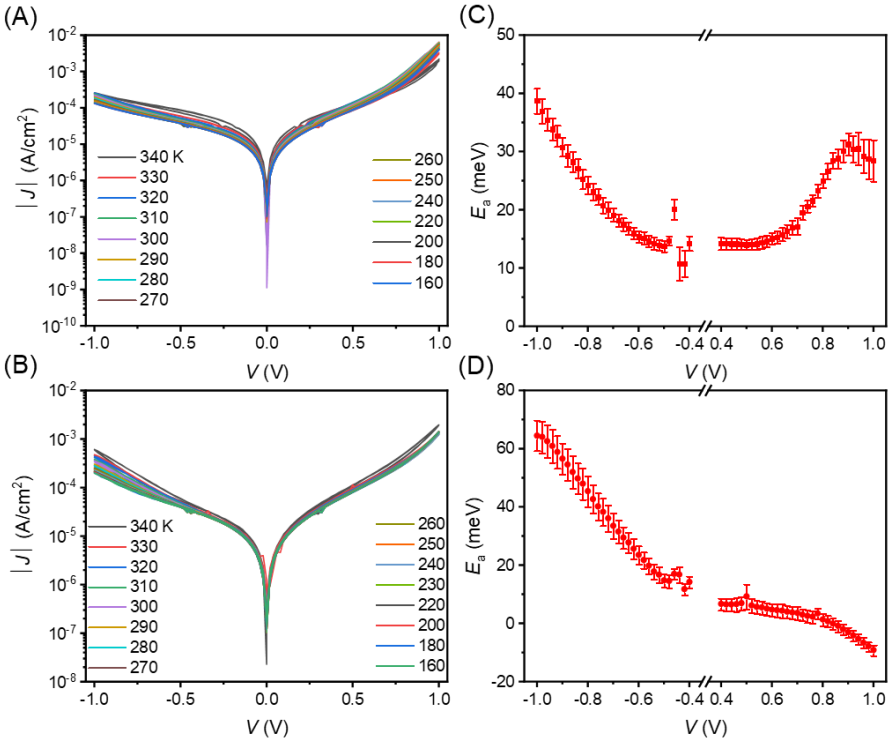

Figure S16: $J(V, T)$ data for (A) Au-linker-ssDNA$_{15}$-Fc//GaO$_x$/EGaIn and (B) Au-linker-ssDNA$_{30}$-Fc//GaO$_x$/EGaIn junctions for T = 340 to 160 K, respectively. The value of E_a obtained by fitting the $J(V, T)$ data to Eq. 2 as a function of the applied bias (fit is shown in Fig. S19) for ssDNA$_{15}$ (C) and ssDNA$_{30}$ (D), respectively. The error was obtained from Arrhenius fits for 3 scans on a junction.

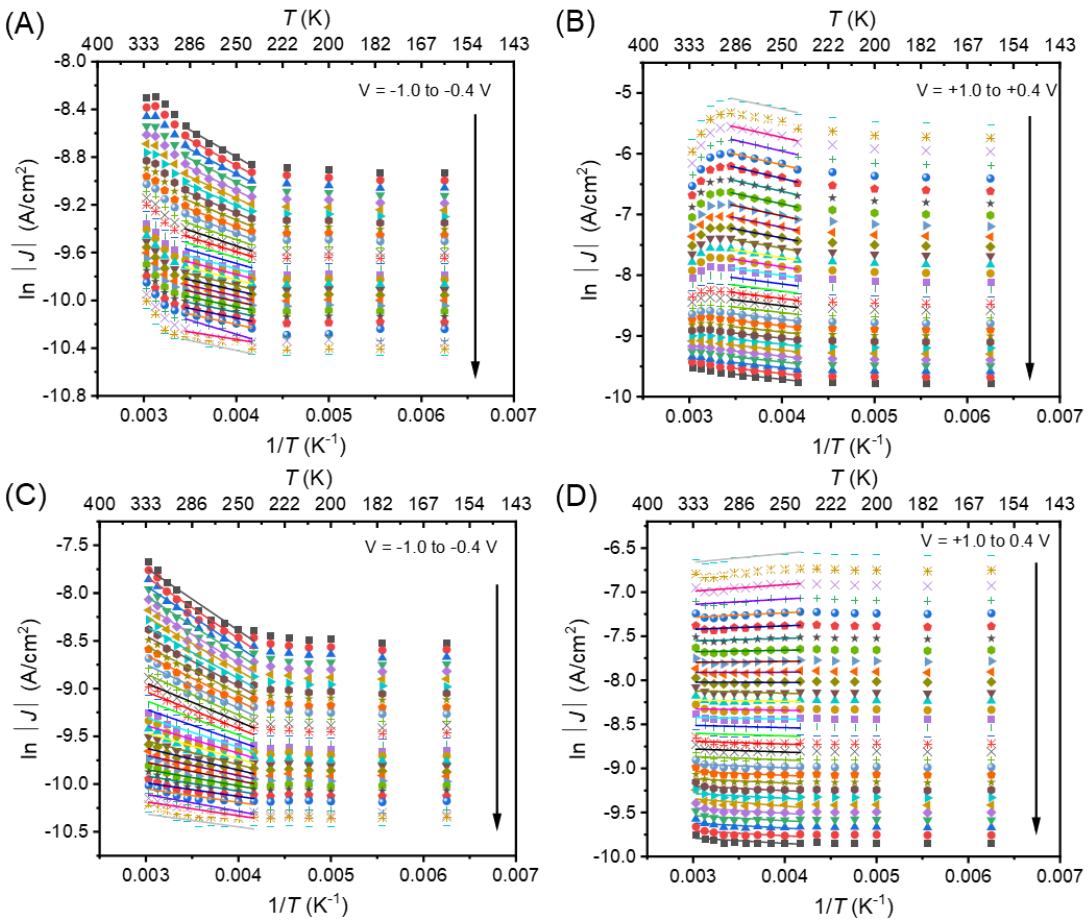

Figure S17: Arrhenius plots for ssDNA$_{15}$ at (A) negative bias and (B) positive bias in ± (0.4 - 1.0) V bias window and for ssDNA$_{30}$ at (C) negative bias and (D) positive bias in ± (0.4 - 1.0) V bias window. The solidlines represent fits to Eq. (2).

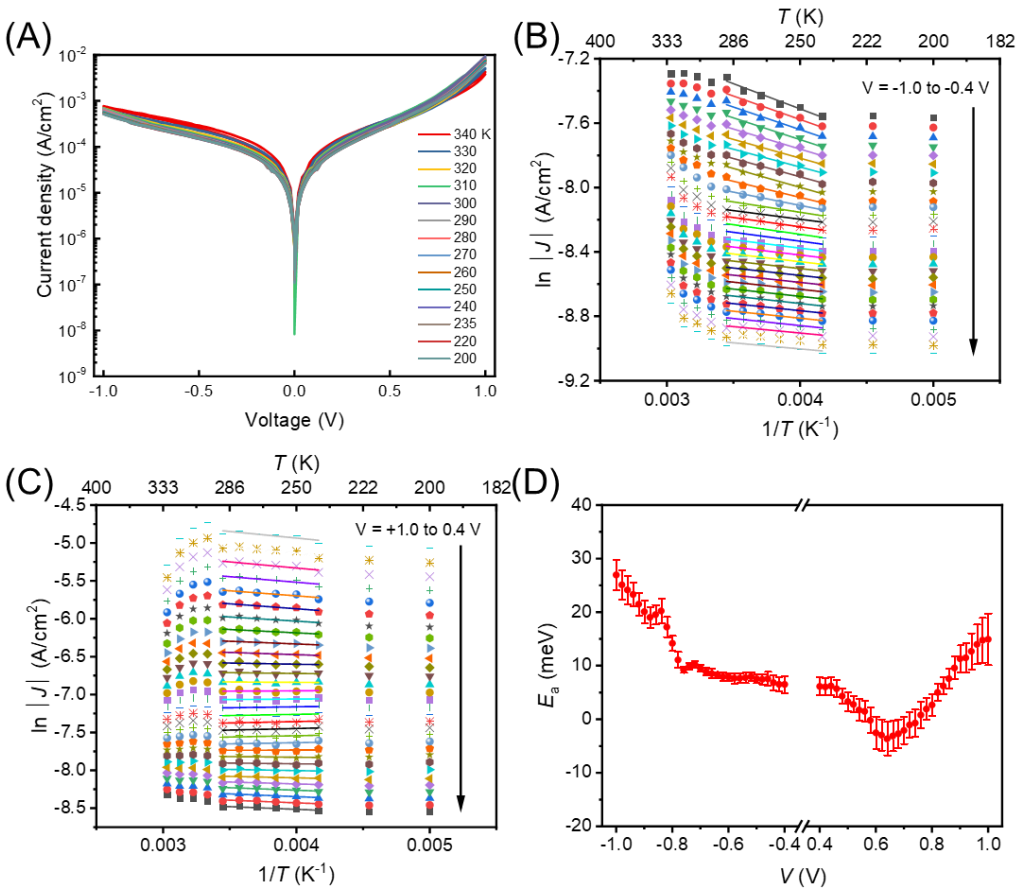

Figure S18: An additional data set for junctions of ssDNA$_{15}$. (A) $J(V,T)$ data for Au-linker-ssDNA$_{15}$-Fc//GaO$_x$/EGaIn for T = 340 – 200 K, (B) Arrhenius plots for V = -0.4 – -1.0 V, (C) Arrhenius plots for V = +0.4 – +1.0 V, and (D) E_a as a function of the applied bias for V = ± (0.4 – 1.0 V).

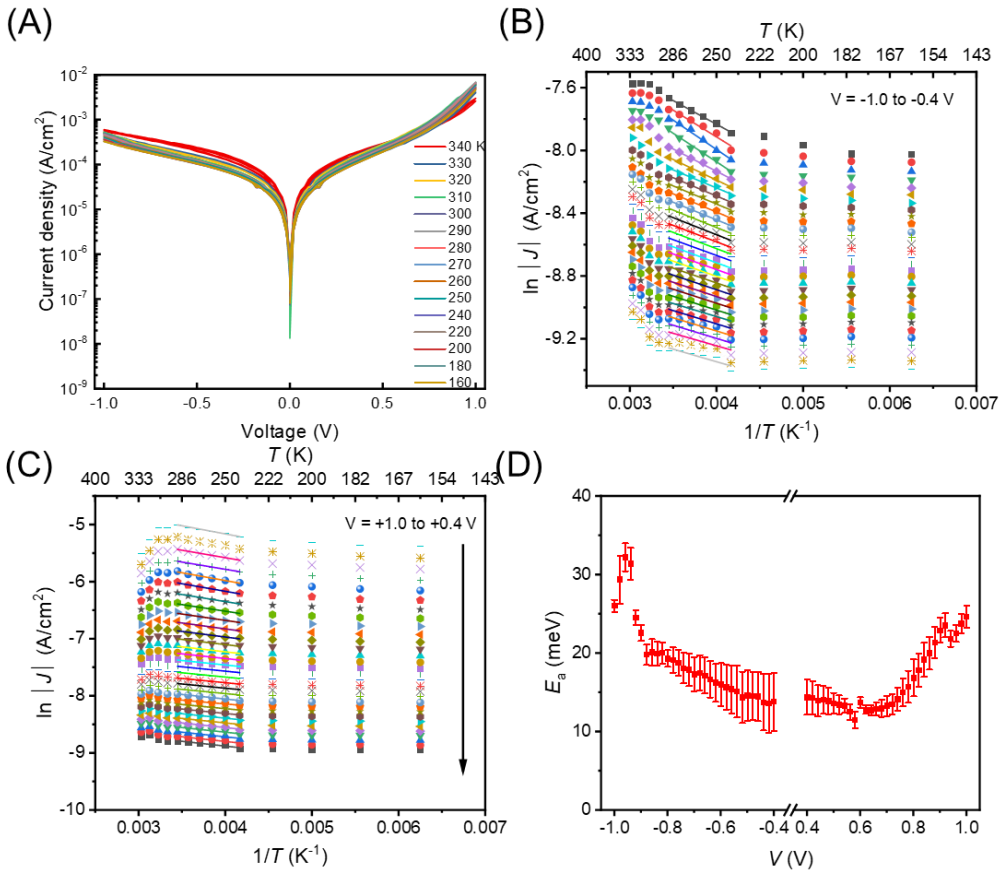

Figure S19: An additional data set for junction of ssDNA$_{15}$, (A) $J(V,T)$ data for Au-linker-ssDNA$_{15}$-Fc//GaO$_x$/EGaIn for T = 340 – 160 K, (B) Arrhenius plots for V = -0.4 – -1.0 V, (C) Arrhenius plots for V = +0.4 – -1.0 V, and (D) E_a as a function of the applied bias for V = ± (0.4 – 1.0 V).

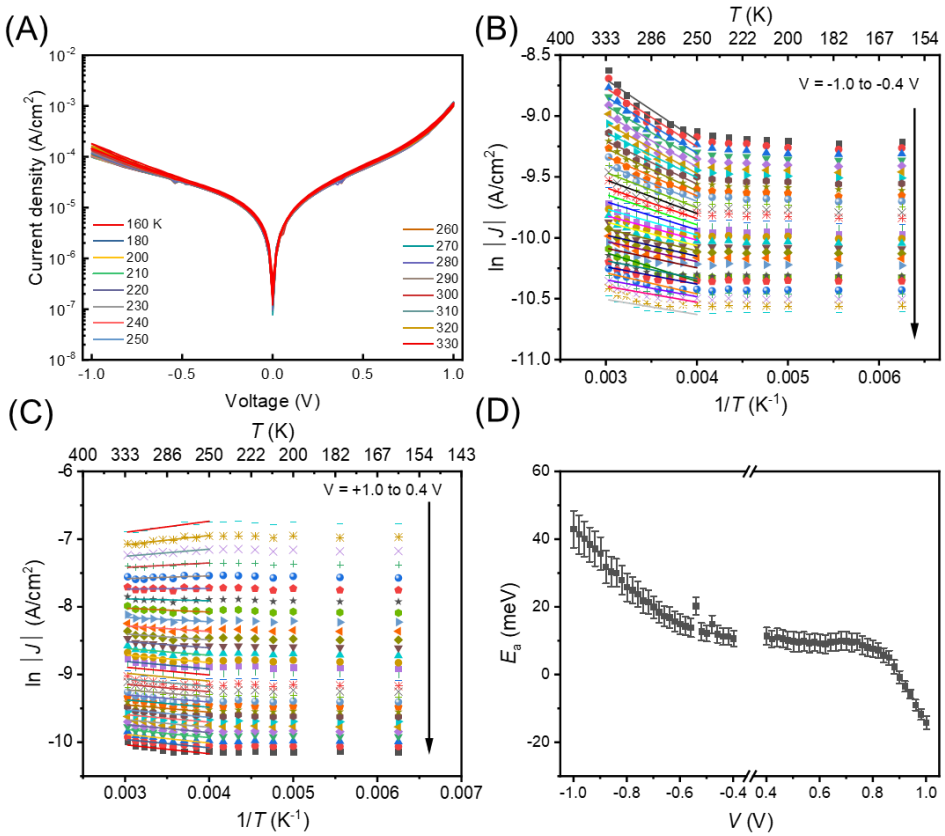

Figure S20: An additional dataset for junction of ssDNA$_{30}$ (A) $J(V,T)$ data for Au-linker-dsDNA$_{30}$-Fc//GaO$_x$/EGaIn tunnel junction for T = 340 – 150 K, (B) Arrhenius plots for V = -0.4 – -1.0 V, (C) Arrhenius plots for V = +0.4 – -1.0 V, and (D) E_a as a function of the applied bias for V = ± (0.4 – 1.0 V).

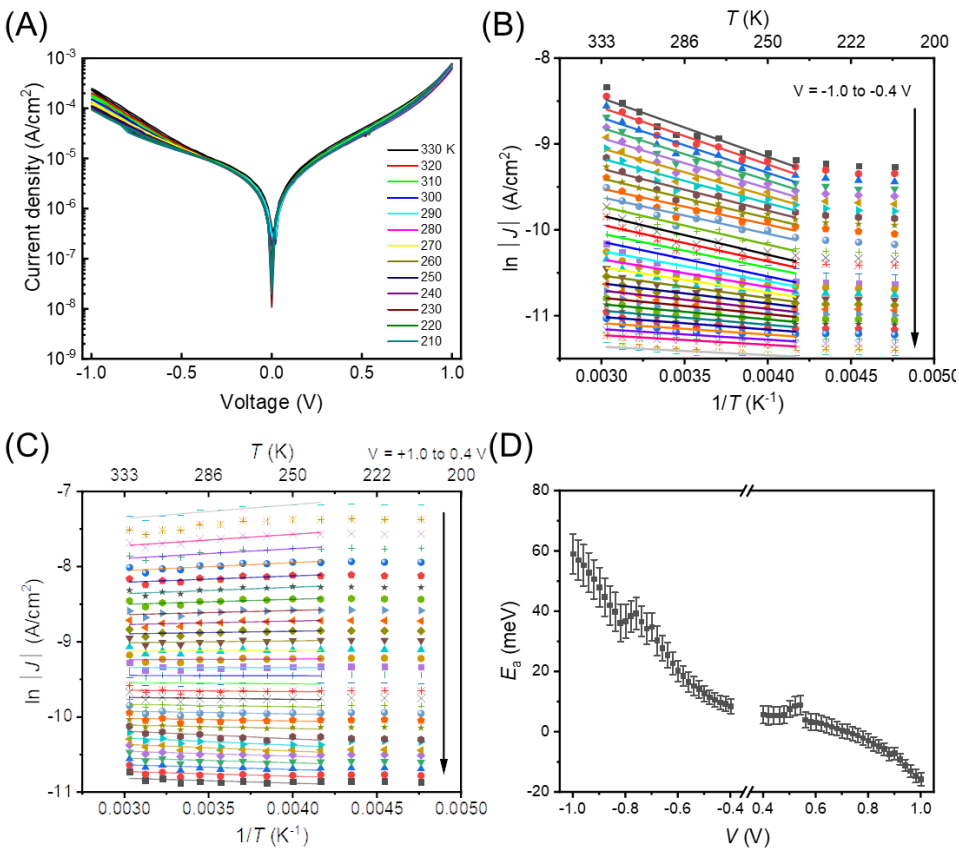

Figure S21: An additional dataset for junction of ssDNA$_{30}$ (A) $J(V,T)$ data for Au-linker-dsDNA$_{30}$-Fc//GaO$_x$/EGaIn tunnel junction for T = 340 – 210 K, (B) Arrhenius plots for V = -0.4 – -1.0 V bias range, (C) Arrhenius plots for V = +0.4 – +1.0 V bias range, and (D) E_a as a function of the applied bias for V = ± (0.4 – 1.0 V).

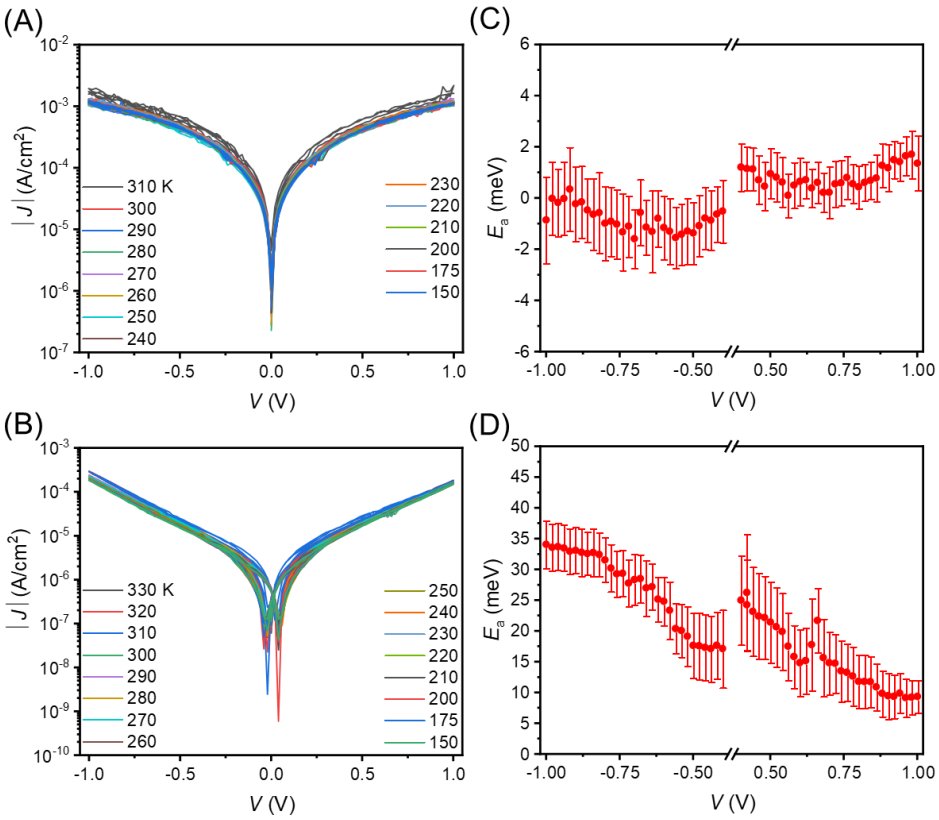

Figure S22: $J(V,T)$ data for (A) Au-linker-dsDNA$_{15}$-Fc//GaO$_x$/EGaIn and (B) Au-linker-dsDNA$_{30}$-Fc//GaO$_x$/EGaIn tunnel junctions for T = 310 – 160 K and T = 330 – 150 K, respectively. The value of E_a plotted as a function of V. The error bar represents the error obtained from the Arrhenius fits.

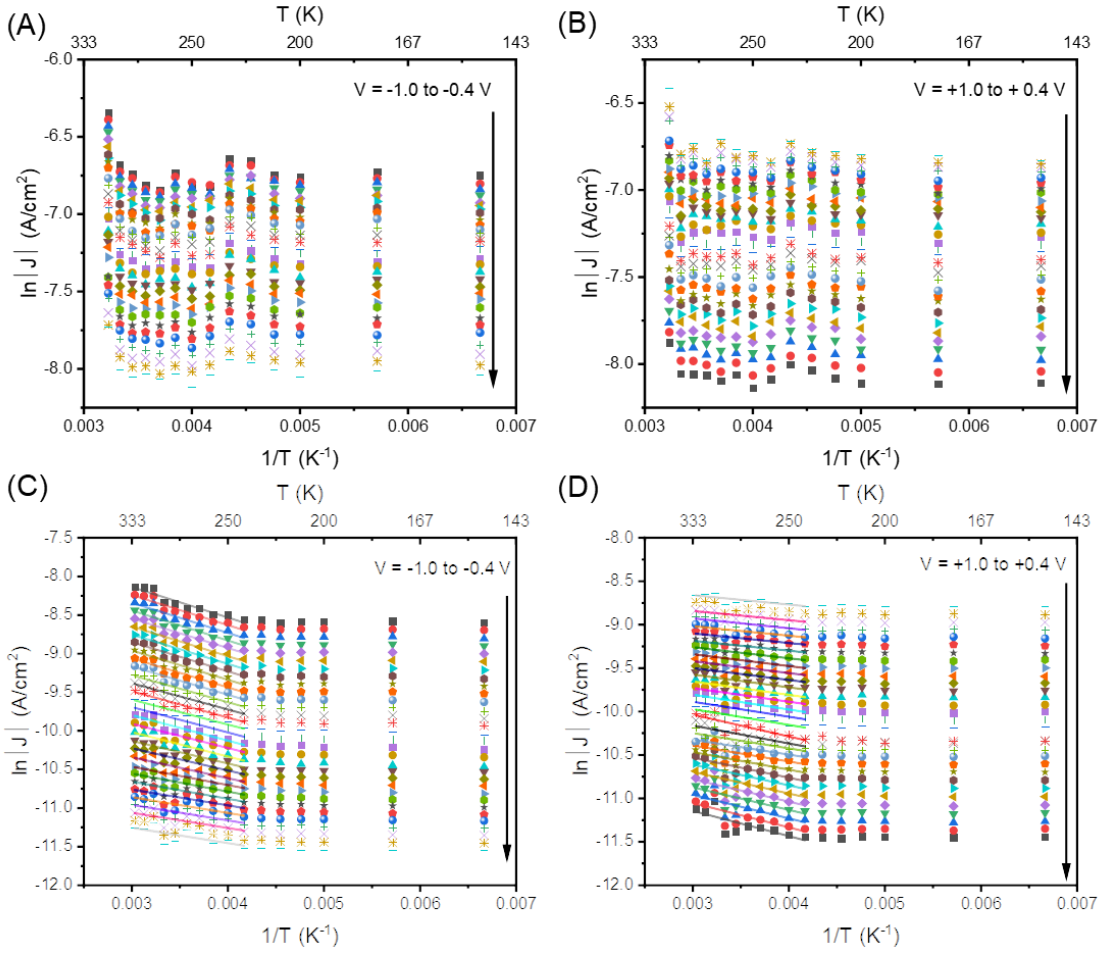

Figure S23: Arrhenius plots obtained for junctions with $dsDNA_{15}$ for V = +0.4 - +1.0 (A) and V = -0.4 to -1.0 (B), the same but for junctions with $dsDNA_{30}$ (C and D).

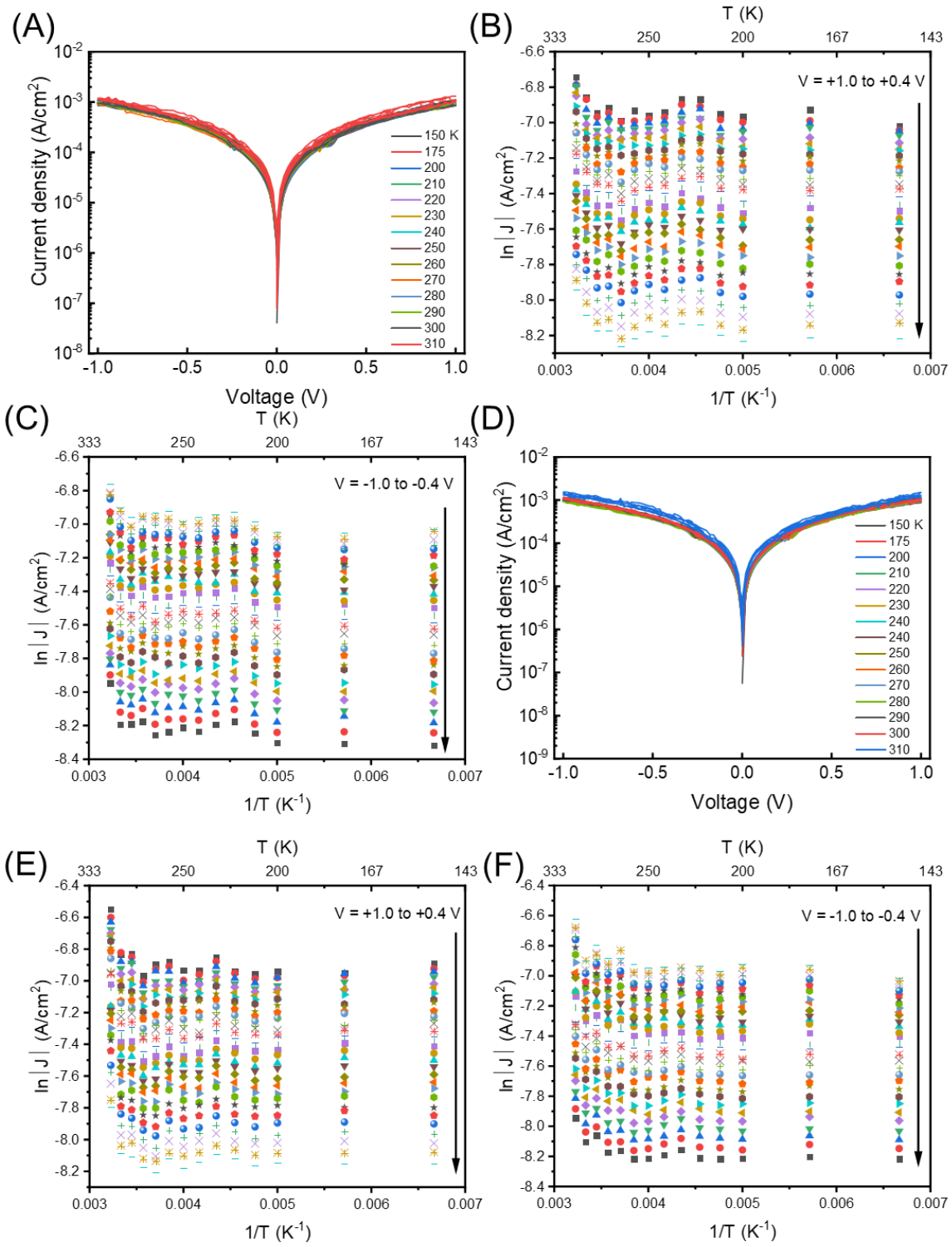

Figure S24: Two more junctions for $dsDNA_{15}$, (A) and (D) $J(V,T)$ data for Au-linker-$dsDNA_{15}$-Fc//GaO_x/EGaIn for the temperature range 310 to 150 K, (B) and (E) Arrhenius plots for V = +0.4 – +1.0 V, (C) and (F) Arrhenius plots for V = -0.4 – -1.0 V as a function of the applied bias for V = ± (0.4 – 1.0 V).

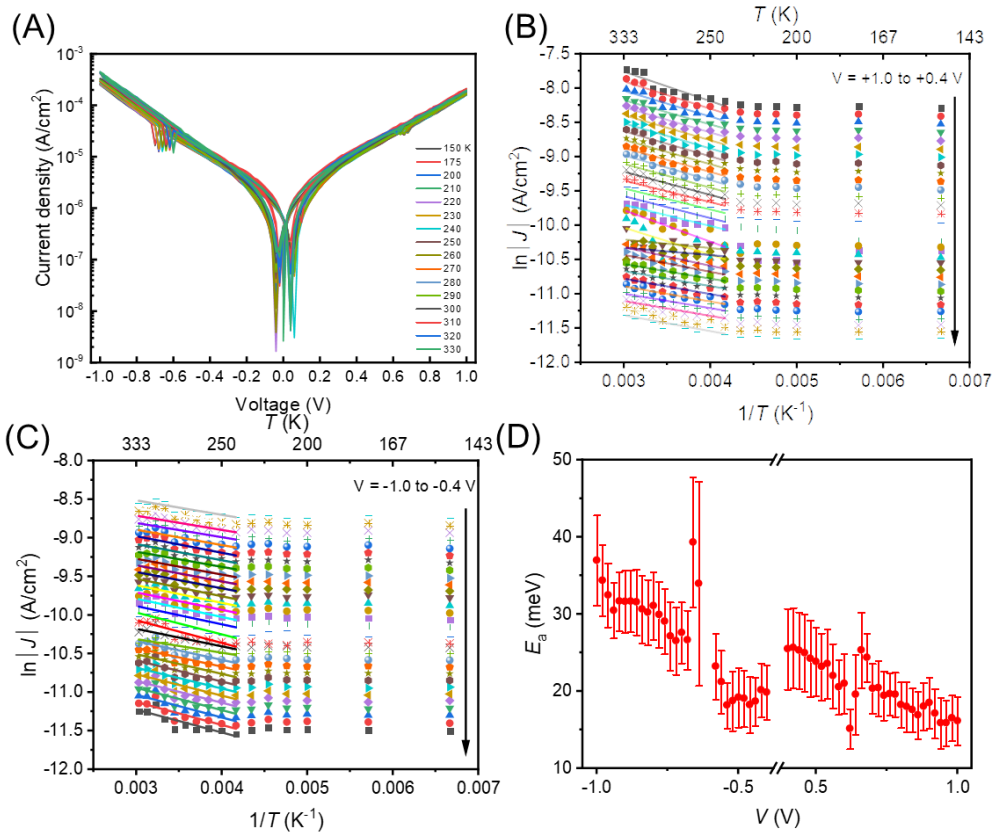

Figure S25: Data obtained from an additional junction with dsDNA$_{30}$. (A) $J(V,T)$ data for Au-linker-dsDNA$_{30}$-Fc//GaO$_x$/EGaIn tunnel junction, for T = 330 to 150 K, (B) Arrhenius plots for V = +0.4 to +1.0 V, (C) Arrhenius plots for V = -0.4 to -1.0 V bias range, (D) E_a as a function of the applied bias for V = ± (0.4 – 1.0 V).

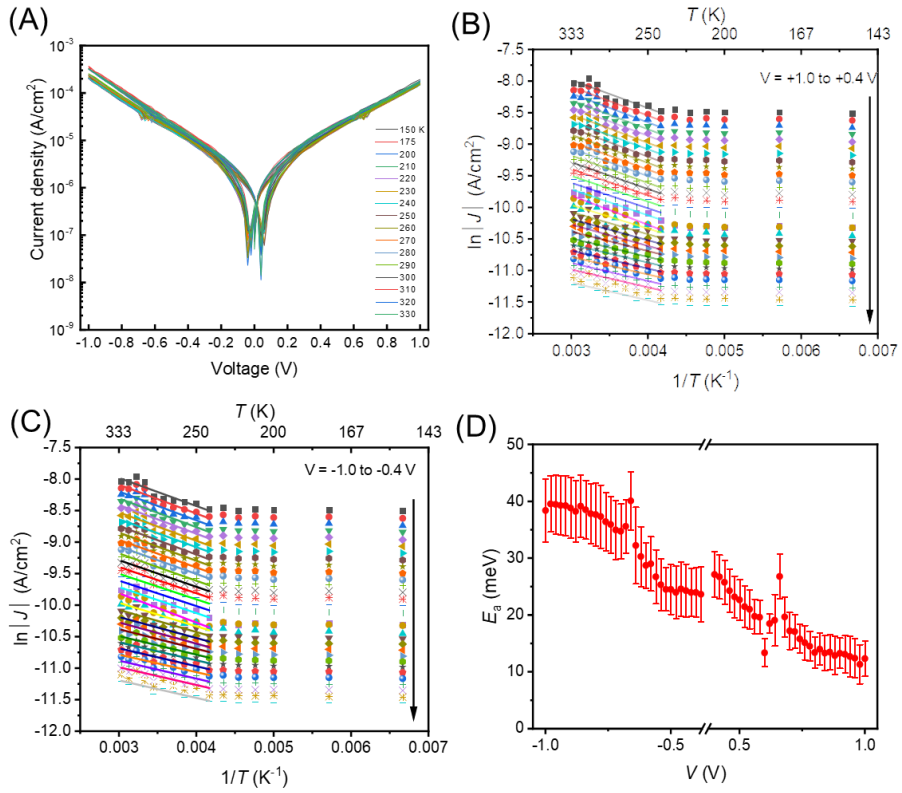

Figure S26: Data obtained from an additional junction with $dsDNA_{30}$. (A) $J(V,T)$ data for Au-linker-$dsDNA_{30}$-Fc//GaO_x/EGaIn junction for T = 330 to 150 K, (B) Arrhenius plots for V = +0.4 to +1.0 V, (C) Arrhenius plots for V = -0.4 to -1.0 V, (D) E_a as a function of V.

S3.10 Melting point estimation

The melting point calculations of $dsDNA_{15}$ and $dsDNA_{30}$ were performed using the online DNA calculator at http://biotools.nubic.northwestern.edu/OligoCalc.html.

The Tm values provided were not salt adjusted as this most closely represents the conditions present in the junction during the $J(V,T)$ measurements.

S4: References:

(1) Ihara, T.; Sasahara, D.; Shimizu, M.; Jyo, A. DNA Conjugates Bearing a Ferrocenyl Group in Backbone and Their Electrochemical Behaviour. *Supramol. Chem.* **2009**, *21* (3–4), 207–217. https://doi.org/10.1080/10610270802468405.

(2) Yuan, L.; Jiang, L.; Zhang, B.; Nijhuis, C. A. Dependency of the Tunneling Decay Coefficient in Molecular Tunneling Junctions on the Topography of the Bottom Electrodes. *Angew. Chemie - Int. Ed.* **2014**, *53* (13), 3377–3381. https://doi.org/10.1002/anie.201309506.

(3) Vilar, M. R.; Botelho do Rego, A. M.; Ferraria, A. M.; Jugnet, Y.; Noguès, C.; Peled, D.; Naaman, R. Interaction of Self-Assembled Monolayers of DNA with Electrons: HREELS and

XPS Studies. *J. Phys. Chem. B* **2008**, *112* (23), 6957–6964. https://doi.org/10.1021/jp8008207.
(4) Jiang, L.; Yuan, L.; Cao, L.; Nijhuis, C. A. Controlling Leakage Currents: The Role of the Binding Group and Purity of the Precursors for Self-Assembled Monolayers in the Performance of Molecular Diodes. *J. Am. Chem. Soc.* **2014**, *136* (5), 1982–1991. https://doi.org/10.1021/ja411116n.
(5) Elhadj, S.; Singh, G.; Saraf, R. F. Optical Properties of an Immobilized DNA Monolayer from 255 to 700 Nm. *Langmuir* **2004**, *20* (13), 5539–5543. https://doi.org/10.1021/la049653+.
(6) Legay, G.; Markey, L.; Meunier-Prest, R.; Finot, E. Measurements of Thickness Dispersion in Biolayers by Scanning Force Microscopy and Comparison with Spectroscopic Ellipsometry Analysis. *Ultramicroscopy* **2007**, *107* (10–11), 1111–1117. https://doi.org/10.1016/j.ultramic.2007.02.043.
(7) Katsouras, I.; Piliego, C.; Blom, P. W. M.; de Leeuw, D. M. Transverse Charge Transport through DNA Oligomers in Large-Area Molecular Junctions. *Nanoscale* **2013**, *5* (20), 9882. https://doi.org/10.1039/c3nr03183g.
(8) Gray, D. E.; Case-Green, S. C.; Fell, T. S.; Dobson, P. J.; Southern, E. M. Ellipsometric and Interferometric Characterization of DNA Probes Immobilized on a Combinatorial Array. *Langmuir* **1997**, *13* (10), 2833–2842. https://doi.org/10.1021/la962139m.
(9) Nerngchamnong, N.; Yuan, L.; Qi, D.-C.; Li, J.; Thompson, D.; Nijhuis, C. A. The Role of van Der Waals Forces in the Performance of Molecular Diodes. *Nat. Nanotechnol.* **2013**, *8* (2), 113–118. https://doi.org/10.1038/nnano.2012.238.
(10) Nijhuis, C. A.; Reus, W. F.; Barber, J. R.; Dickey, M. D.; Whitesides, G. M. Charge Transport and Rectification in Arrays of SAM-Based Tunneling Junctions. *Nano Lett.* **2010**, *10* (9), 3611–3619. https://doi.org/10.1021/nl101918m.